

# **X-ray photoelectron spectroscopy (XPS) of Quinacridone (QA) on Ag(100) surface**

## **Focusing Laboratory Course**

Lucas Hirschfeld

Clausius Institute for Physical and Theoretical Chemistry University of Bonn

Research group of Prof. Dr. Moritz Sokolowski

Bonn 2025



# Contents

<b>1</b>	<b>Introduction</b>	<b>1</b>
<b>2</b>	<b>Literature</b>	<b>3</b>
2.1	Structures of QA on the Ag(100) surface . . . . .	3
<b>3</b>	<b>Theory</b>	<b>5</b>
3.1	X-ray photoelectron spectroscopy (XPS) . . . . .	5
<b>4</b>	<b>Experimental</b>	<b>7</b>
4.1	Material . . . . .	7
4.1.1	Ag(100) crystal . . . . .	7
4.1.2	Quinachridone (QA) . . . . .	8
4.2	Experimental setup . . . . .	9
4.3	Data processing . . . . .	10
<b>5</b>	<b>Results</b>	<b>13</b>
5.1	The 1D $\alpha$ -Phase . . . . .	13
5.1.1	C1s spectra . . . . .	14
5.1.2	O1s spectra . . . . .	17
5.1.3	N1s spectra . . . . .	21
5.2	C1s XPS spectra for the phase transition . . . . .	25
5.3	The commensurate 2D $\beta$ -Phase . . . . .	27
5.3.1	C1s spectra . . . . .	27
5.3.2	O1s spectra . . . . .	31
5.3.3	N1s spectra . . . . .	33
5.4	Binding energy changes upon phase transition . . . . .	35
<b>6</b>	<b>Discussion</b>	<b>37</b>
6.1	The 1D $\alpha$ -Phase . . . . .	37
6.2	Phase transition . . . . .	38
6.3	The commensurate 2D $\beta$ -Phase . . . . .	38
<b>7</b>	<b>Summary and Outlook</b>	<b>43</b>
<b>8</b>	<b>Appendix</b>	<b>45</b>
	List of abbreviations . . . . .	49
	<b>Bibliography</b>	<b>50</b>



# 1 Introduction

The examination of surfaces and adsorbates is essential for endless disciplines, each offering unique insights and applications. A broad array of disciplines is encompasses within these fields, which include but are not limited to: coatings, electronic, nanotechnology, energy and transportation.<sup>[1]</sup> Furthermore, the relevance of surface science to environmental degradation and corrosion has been well-documented.<sup>[2]</sup> In order to be applicable in these fields, it is necessary that the surfaces and the adsorbates possess particular characteristics, such as well-defined structure or a high dipole moment. For instance, the utilization of specific organic adsorbates has facilitated the development of innovative organic solar cells, which exhibit a high degree of flexibility.<sup>[3–5]</sup>

One molecule that merits particular attention in the context of these applications is quinachridone (QA). It has been established that the molecule in question is capable of forming one-dimensional (1D) molecular chains within its bulk crystal structure<sup>[6]</sup> and on surfaces,<sup>[7–10]</sup> with these chains being connected via intermolecular hydrogen bonds.

In previous studies, the potential of QA for application in electronic devices has been demonstrated.<sup>[11–13]</sup> Its potential extends beyond the domain of printer toners, where it is generally employed, offering significant promise for applications in diverse fields. Examples of applications for QA are organic field-effect transistors (OFETs),<sup>[14–17]</sup> organic light-emitting diodes (OLEDs)<sup>[18–20]</sup> and organic photovoltaics (OPVs).<sup>[21,22]</sup> The subsequent exploration of the structural characteristics of QA on metal surfaces, such as silver (Ag), is driven by the promising properties. This work represents a continuation of the previous examination conducted by N. Humberg, which investigated the different structures of QA on the Ag(100) surface.<sup>[10]</sup>

The utilization of alternative techniques, specifically x-ray photoelectron spectroscopy (XPS), in comparison to previous methods will facilitate a more detailed comprehension of the structure of QA on the Ag(100) surface. This, in turn, will lead to the identification of additional properties inherent to this adsorbate-substrate system.



## 2 Literature

### 2.1 Structures of QA on the Ag(100) surface

In principle, two primary structures are observed to form on the Ag(100) surface: the  $\alpha$ - and  $\beta$ -Phase. A thorough examination of these two phases has been conducted by N. Humberg.<sup>[10]</sup>

It has been ascertained that the formation of the  $\alpha$ -phase occurs subsequent to the deposition of the QA molecules onto the Ag(100) surface at a sample temperature of 300 K. This phase is composed of domains of parallel molecular chains that are flat-lying on the surface. The QA molecules are connected via intermolecular hydrogen bonds between the keto groups of one molecular chain and the amine groups of another. It was also determined that the domains under consideration are homochiral, a finding that suggests a high degree of mobility for the QA molecules on Ag(100) at 300 K. In addition, the superstructure matrix of the  $\alpha$ -phase was determined using a spot profile analysis low energy electron diffraction (SPA-LEED) image and scanning tunneling microscopy (STM) results. The following superstructure matrix was found

$$\mathbf{M}_\alpha = \begin{pmatrix} 2 & 1.25 \\ -3 & 4.80 \end{pmatrix},$$

which shows that the structure is of the point-on-line (POL) type.

The phase transition from the  $\alpha$ -phase to the  $\beta$ -phase was discovered when the sample was heated up to 500 K for 15 minutes. The phase transition is irreversible. This means that the  $\alpha$ -phase is metastable and is stabilized by a kinetic barrier from the intermolecular hydrogen bonds.

For the  $\beta$ -phase, the investigation revealed parallel molecular chains, which are comprised of dimers and manifest periodic indents. This results in a single hydrogen bond between the dimers instead of theoretical two possible hydrogen bonds. The two molecules of the dimer form two hydrogen bonds with each other. Once more, employing a SPA-LEED image and STM results, the superstructure matrix of the  $\beta$ -phase was determined as

$$\mathbf{M}_\beta = \begin{pmatrix} 4 & 3 \\ -5 & 3 \end{pmatrix},$$

which means that the structure is commensurate. The structure of the  $\alpha$ - and  $\beta$ -phase corresponding to the structure model of N. Humberg is illustrated in Figure 2.1.

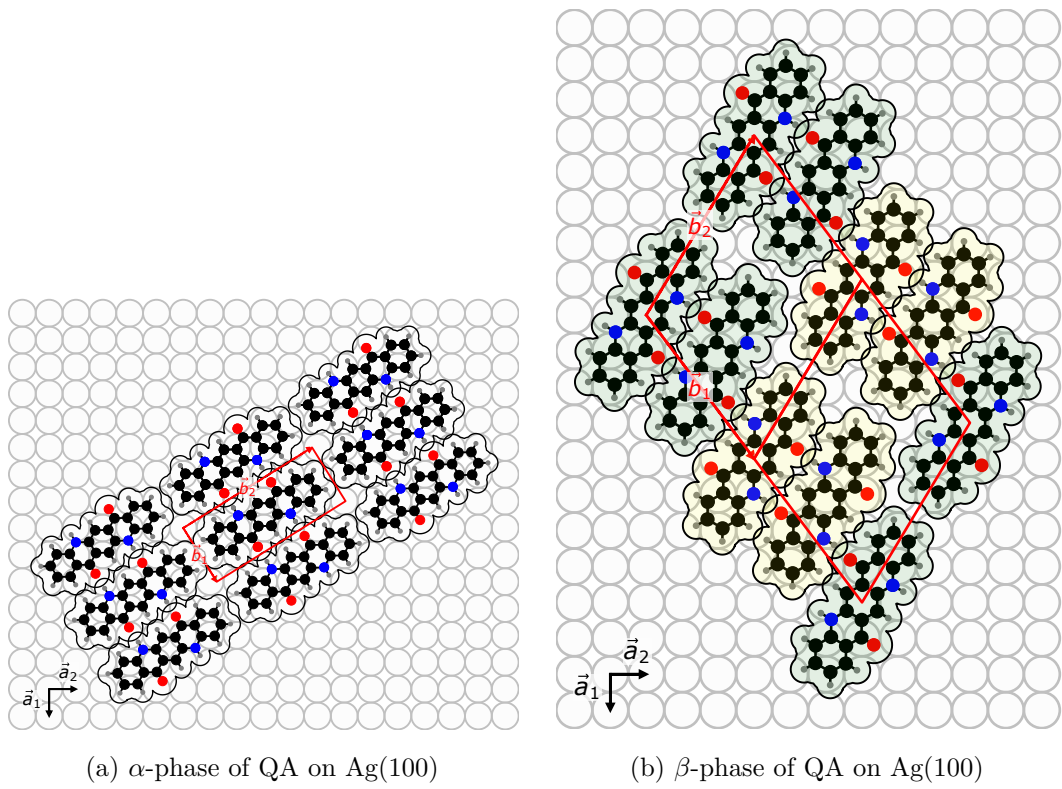


Figure 2.1: Structure models for the  $\alpha$ - and the  $\beta$ -phase of QA on Ag(100) according to the literature [10].

# 3 Theory

## 3.1 X-ray photoelectron spectroscopy (XPS)

X-ray photoelectron spectroscopy (XPS) is one of the different types of electron spectroscopy where an excitation leads to the ejection of an electron from a bound state to the continuum, called the photoelectric effect.<sup>[23,24]</sup> The photons of x-rays have similar energy as the binding energies (BEs) of deep core electrons and are therefore used for the excitation. One can divide x-rays for surface science into two different categories: soft (100 - 2100 eV) and hard x-rays ( $> 2100$  eV).

When an atom absorbs one of these photons, a photoelectron, which has a characteristic energy corresponding to the atom and its bonding environment, is emitted. The change of energy due to the bonding environment and its oxidation state is called chemical shift.<sup>[25]</sup> A schematic drawing of this process is illustrated in Figure 3.1

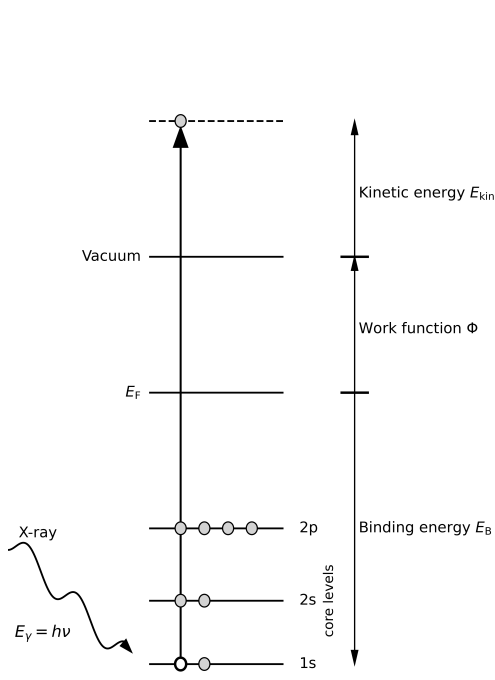


Figure 3.1: Schematic drawing of the photoemission process of an electron in the 1s orbital upon x-ray excitation. The image has been illustrated using reference [26].

The kinetic energy of the photoelectron  $E_{\text{kin}}$ , that is referenced against the Fermi level  $E_F$  for solid substrates by convention, is given by:<sup>[27,28]</sup>

$$E_{\text{kin}} = h\nu - E_B, \quad (3.1)$$

where  $E_B$  denotes the binding energy (BE) of the photoelectron. Without referencing against  $E_F$ , one would also take the work function of the sample  $\phi_{\text{sample}}$  into account:

$$E_{\text{kin}} = h\nu - E_B - \phi_{\text{sample}}. \quad (3.2)$$

The BE  $E_B$  of an electron is defined as the difference in energies between the atom with  $n$  electrons and the ion with  $n - 1$  electrons:

$$E_B = E_f(n - 1) - E_i(n), \quad (3.3)$$

As seen in this equation, the BE of photoelectrons depends on initial and final state effects. The initial state effects manifest for the neutral unexcited atom, due to its interaction with its immediate electronic environment, also referred to as the chemical environment. In addition, final state effects emerge from the correlation between the photoemission process and the ionized final state. The rapid nature of the photoemission process may preclude the system from attaining adiabatic equilibrium.<sup>[27]</sup>

The final state effects are characterized by the presence of satellites with reduced kinetic energy, correlating to increased BE. This is exemplified by phenomena such as shake-up lines or asymmetric line shapes of the signal, which are indicative of photoemission from the metal surface. The asymmetric line shapes result from coupling of the photoelectrons to the conduction electrons.<sup>[29]</sup> A multitude of factors have been identified as contributors to the line shape, particularly the Full Width at Half Maximum (FWHM), of the photoemission lines. These include phonon broadening, the lifetime of the photohole, the spectral resolution of the exciting x-ray beam and the energy resolution of the analyzer.<sup>[29,30]</sup>

# 4 Experimental

## 4.1 Material

### 4.1.1 Ag(100) crystal

A silver (Ag) single crystal from the Diamond Light Source with a crystal orientation of (100) was used as the adsorbent for the XPS experiments. It is important that a single crystal is used, as this has a uniform and precisely defined surface and has almost no structural defects.

Silver forms a face-centered cubic (fcc) crystal system, which is shown in Figure 4.1. This corresponds to the Pearson symbol cF. In the crystal system of silver, one silver atom is surrounded by twelve others. Furthermore, Ag(100) does not reconstruct. The lattice constant of silver in volume is  $4.0862 \pm 0.0002 \text{ \AA}$  at a temperature of  $25 \pm 5 \text{ }^{\circ}\text{C}$ .<sup>[31,32]</sup>

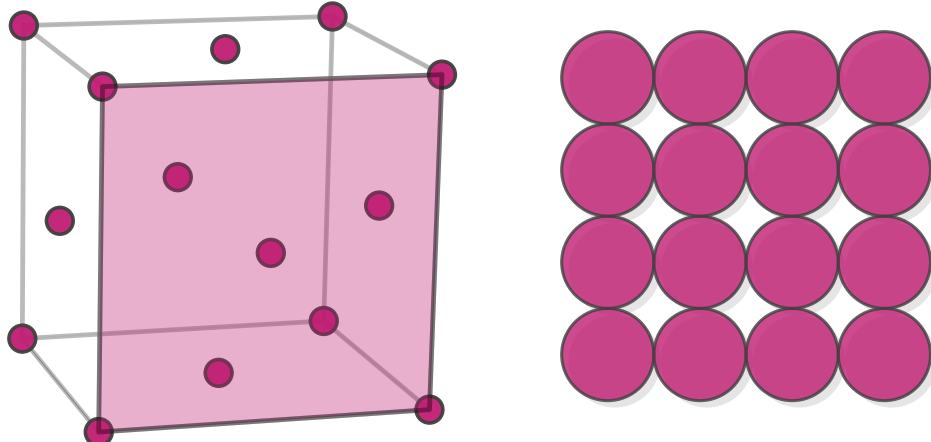


Figure 4.1: Unit cell of the silver crystal with marked (100) plane and the surface of Ag(100).

As seen in Figure 4.1, the surface of the Ag(100) single crystal has a quadratic shape with the lattice constant  $4.0862 \text{ \AA}/\sqrt{2} = 2.8894 \text{ \AA}$ . The surface has different adsorption sites called fcc, on-top and bridge.

#### 4.1.2 Quinachridone (QA)

The examined adsorbate quinachridone (QA) is a high symmetric, red colored organic molecule with the full IUPAC name 5,12-dihydro-quino[2,3-*b*]acridine-7,14-dione and the sum formula C<sub>20</sub>H<sub>12</sub>N<sub>2</sub>O<sub>2</sub>. QA is most prominently recognized as the parent structure of a group of pigments, most notably Pigment Violet 19 (C.I. 73900). This particular pigment is extensively utilized in industrial applications due to its remarkable color properties and stability.<sup>[33,34]</sup> The molecular structure of QA is shown in Figure 4.2.

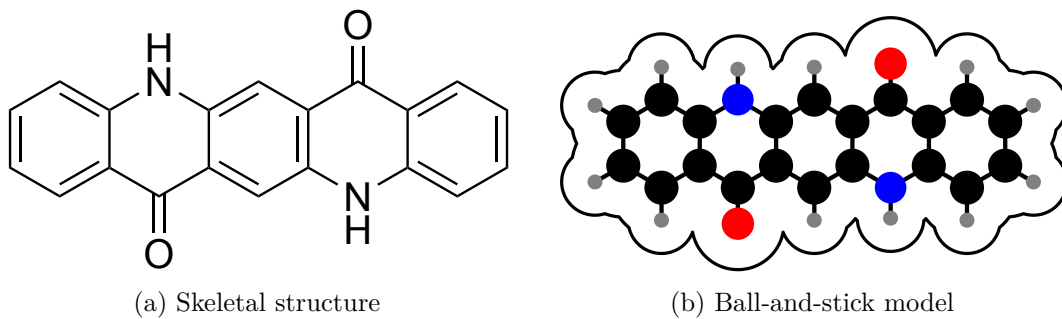


Figure 4.2: Molecular structure of quinachridone (QA).

The molecule is classified as a heterocyclic compound. Its structure is characterized by a conjugated ring system that imparts significant rigidity and planarity to the molecule.<sup>[35]</sup> QA is of the symmetry group C<sub>2h</sub> and has a molar mass of 312.32 g/mol. The molecule is a crystalline solid with four known different crystal structures under standard conditions.<sup>[6,36]</sup>

## 4.2 Experimental setup

All XPS measurements were performed in an ultra-high vacuum (UHV) chamber at the I09 endstation at the Diamond Light Source in Didcot, UK, which is depicted in Figure 4.3.

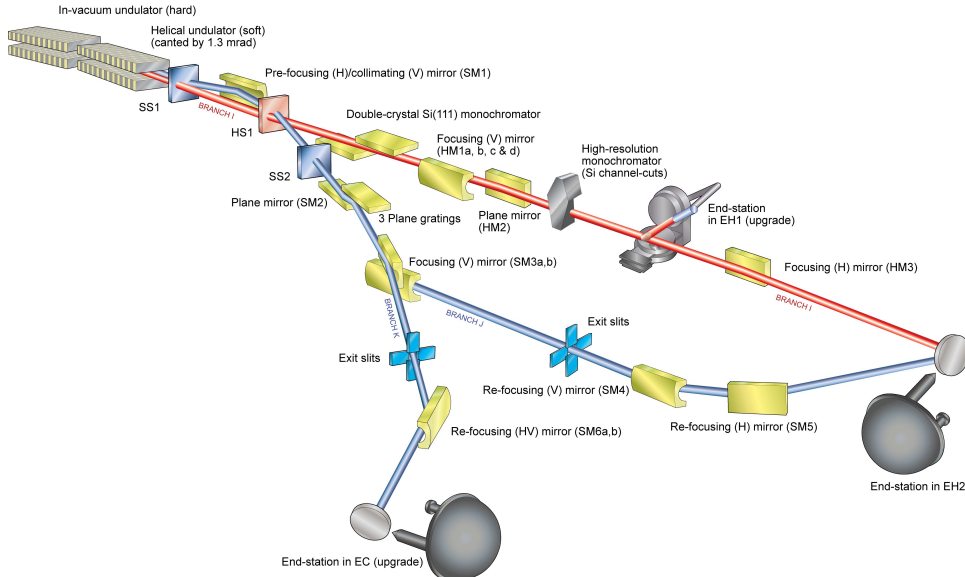


Figure 4.3: Schematic drawing of the I09 endstation of the Diamond Light Source in Didcot, UK. Picture taken from [37].

This particular endstation utilizes radiation from an undulator located inside the electron storage ring of the synchrotron. The I09 endstation is equipped with a nitrogen-cooled Si(111) double crystal monochromator and a grating monochromator. This setup enables high-intensity and precise x-ray measurements in the soft and hard x-ray ranges. The emitted photoelectrons were detected by a hemispherical EW4000 HAXPES analyzer purchased from Scienta Omicron. The analyzer has an acceptance cone of  $56^\circ$  and was mounted in the photon polarization plane.<sup>[37]</sup> A schematic drawing of the measurements position is illustrated in Figure 4.4.

The experimental preparation for the measurements are described in the following. First, the Ag(100) surface is cleaned by sputtering with argon ions. Therefore, argon is dosed into the chamber up to a pressure of  $5 \cdot 10^{-5}$  mbar and is accelerated with a voltage of 1 keV. Afterwards, the surface is heated up to 825 K for 45 min to increase the thermal diffusion and heal defects on the Ag(100) surface. Subsequently, QA was evaporated onto the Ag(100) surface. Therefore, the evaporator was heated to about 500 °C.

For the measurements of the XPS spectra, soft x-ray radiation with an energy of either 500 eV for C1s and N1s or 630 eV for O1s was used. Therefore, the sample is rotated by  $-45^\circ$  in the polar direction toward the analyzer. The detailed parameter for the data acquisition are listed in Table 4.1.

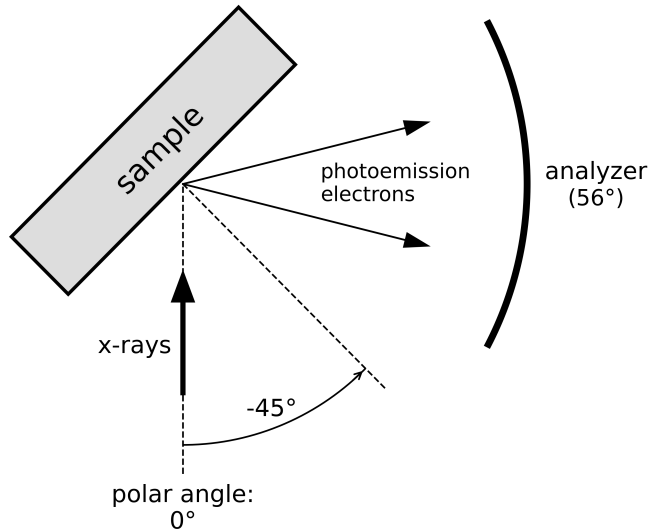


Figure 4.4: Top view of the sample geometries for the XPS measurements at the I09 endstation of the Diamond Light Source in Didcot, UK. Illustrated as in reference [38].

Table 4.1: Experimental parameter for XPS measurements at the I09 endstation of the Diamond Light Source in Didcot, UK.

	photon energy $E_\gamma$	pass energy $E_{\text{pass}}$	step width	number of frames
C1s	500 eV	20 eV	40 meV	17
O1s	630 eV	20 eV	40 meV	17
N1s	500 eV	20 eV	40 meV	17

### 4.3 Data processing

The measured data were then subjected to an initial processing stage, whereby the values from multiple datasets employing identical settings for the measurements were averaged. Subsequently, the data underwent further processing with the software CasaXPS.<sup>[39]</sup> Each XPS spectrum was processed in a consistent manner, as outlined below.

Initially, the BE of the XPS spectrum was calibrated against the Fermi energy  $E_F$ . Small inaccuracies of all measurement devices may lead to inaccuracies in the BE. Therefore, a XPS spectrum of the Fermi edge with same photon energy as the corresponding component XPS spectrum is used and fitted with a Fermi function. Without inaccuracies of the devices,  $E_F$  should be zero and for this reason the obtained Fermi energy is then used for the XPS spectrum of the component to calibrate the BE.

Afterwards, a linear background was fitted to the raw and averaged data. This background is then subtracted for further data processing. Afterwards, the corresponding fitting models from chapter 5 were applied. Therefore, the different peaks with line shape and constraints from Table 4.2 were used. These settings are the same for each processed dataset. Subsequently, the processed data was then exported from CasaXPS and illustrated using a customized python script, enabling the generation of various plots as outlined in chapter 5.

Table 4.2: Used parameter in CasaXPS<sup>[39]</sup> for the different peaks of the XPS spectra of QA on Ag(100) at the I09 endstation of the Diamond Light Source in Didcot, UK.

peak	line shape	area constraint
C <sub>arom</sub>	LA(1,8,800)	10
C <sub>NH</sub>	LA(1,8,800)	4
C <sub>CO</sub>	LA(1,8,800)	4
C <sub>O</sub>	LA(1,8,200)	2
O1	LA(1,8,400)	1 (for $\beta$ -phase)
O <sub>1sat</sub>	LA(1,1,400)	
O2	LA(1,8,400)	1 (for $\beta$ -phase)
O <sub>2sat</sub>	LA(1,1,400)	
N1	LA(1,8,400)	1 (for $\beta$ -phase)
N <sub>1damage</sub>	LA(1,8,400)	
N2	LA(1,8,400)	1 (for $\beta$ -phase)



# 5 Results

The ensuing results will be divided into three categories: the  $\alpha$ -phase (section 5.1), the phase transition (section 5.2) from the  $\alpha$ - to the  $\beta$ -phase and the  $\beta$ -phase (section 5.3). A compendium of all recorded XPS spectra, organized according to the different photoemission lines, is available for perusal in chapter 8.

## 5.1 The 1D $\alpha$ -Phase

The investigation of the  $\alpha$ -phase was conducted on all three available photoemission lines: C1s, O1s and N1s. The ensuing discourse will meticulously examine the  $\alpha$ -phase. Therefore, the present chapter has been subdivided into discrete sections, each dedicated to a specific atom type. Within each section, an overview of all recorded XPS spectra for that particular atom type is provided, along with a more detailed view of a representative XPS spectrum for a monolayer. A comparison will be made between the monolayer and the multilayer XPS spectrum.

### 5.1.1 C1s spectra

Figure 5.1 presents a series of C1s XPS spectra of QA adsorbed on Ag(100), recorded at varying coverages ranging from 0.08 monolayer (ML) to 1 ML. All spectra exhibit a dominant peak in the region around 285 eV, which is consistent across all coverages. Furthermore, a slight shoulder towards lower BEs is visible. Towards higher BEs, the XPS spectra show a more complex pathway with at least one peak.

Despite the overall similarity in the spectra, particularly in peak position and general shape, there are notable differences in intensity and variations in peak broadening as a function of coverage. The most apparent trend is the systematic increase in signal intensity with increasing coverage, indicating a proportional growth in the number of photoemitting carbon atoms due to the accumulation of molecules.

The spectrum with the highest intensity that is not a multilayer spectrum is set to 1 ML. The adsorbed layers of the other spectra are then assigned accordingly. This classification of the coverage is used for all XPS spectra for the  $\alpha$ -phase. From the C1s XPS spectra, it can be concluded that there are different peaks corresponding to the carbon atoms in QA. This will be discussed in more detail below.

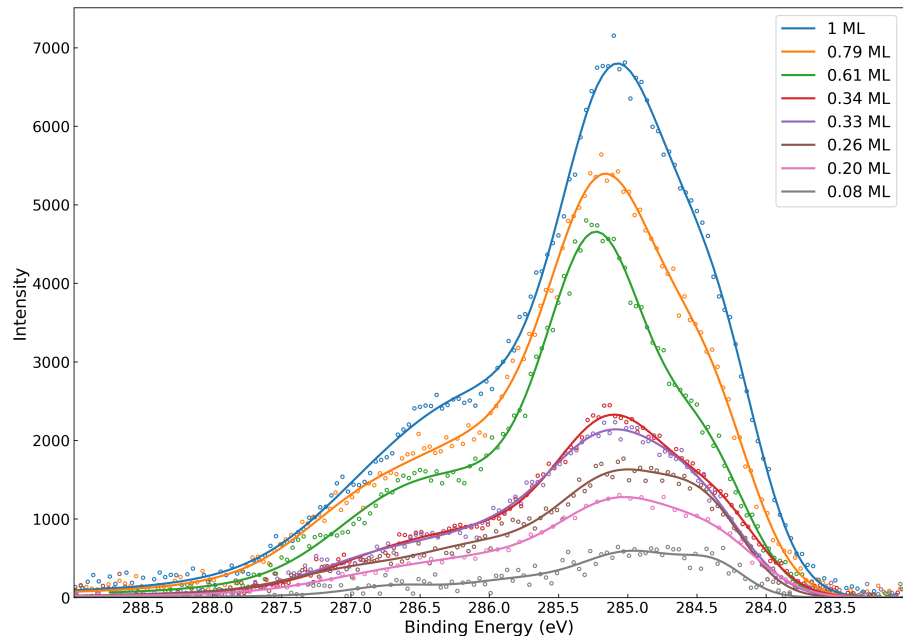


Figure 5.1: Overview of C1s XPS spectra for all preparation of the  $\alpha$ -phase of QA on Ag(100).

The XPS spectrum for a coverage of 1 ML in Figure 5.2 demonstrates different peaks that also present carbon atoms with different chemical environments in QA.

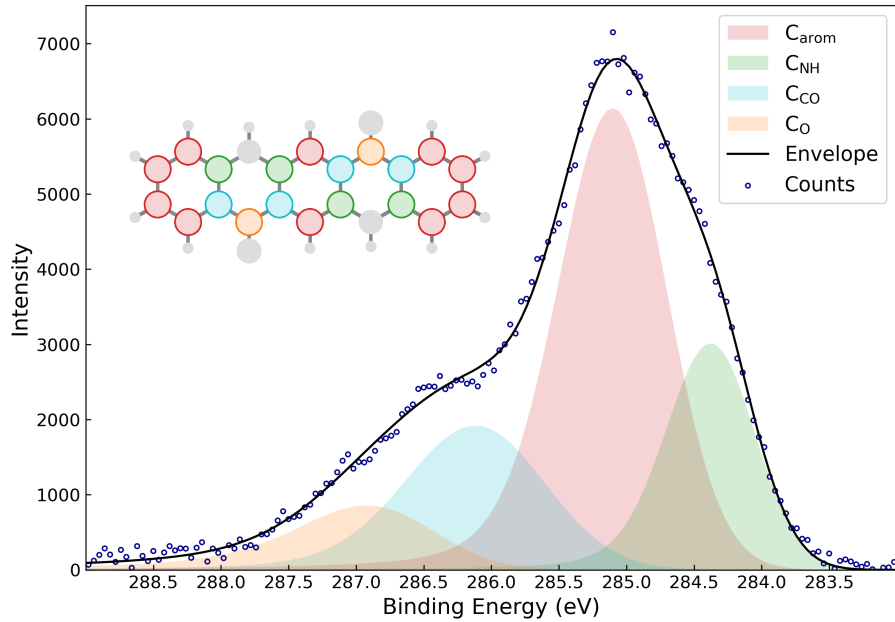


Figure 5.2: C1s XPS spectrum for the  $\alpha$ -phase of QA on Ag(100) for a coverage of 1 ML.

The XPS spectra for the C1s photoemission lines of QA on Ag(100) reveals consistent spectral features. The main peak ( $C_{\text{arom}}$ ) contains the carbon atoms from the aromatic system that are not part of the ring containing the keto and the amine groups. Next, there is a peak for the two atoms next to the amine ( $C_{\text{NH}}$ ) and another peak for the two atoms next to the ketone ( $C_{\text{CO}}$ ). Finally, there is one peak for the carbon atoms of the ketone ( $C_{\text{O}}$ ). The values corresponding to each peak can be found in Table 5.1.

Table 5.1: Fit parameter used in CasaXPS<sup>[39]</sup> for the  $\alpha$ -phase of QA on Ag(100) for the C1s photoemission lines.

peak	BE / eV	area ratio	FWHM / eV
$C_{\text{arom}}$	285.016	10	0.938
$C_{\text{NH}}$	284.308	4	0.764
$C_{\text{CO}}$	286.010	4	1.200
$C_{\text{O}}$	286.723	2	1.152

As illustrated in Figure 5.2 and Table 5.1, the detailed fitting model can be described as follows: The BE of the  $C_{\text{arom}}$  peak is measured at 285.016 eV, with a FWHM of 0.938 eV. The  $C_{\text{NH}}$  peak is next to the aforementioned peak, with a BE of 284.308 eV and a FWHM of 0.764 eV. The analysis of the data reveals that the  $C_{\text{CO}}$  peak is located to the left of the  $C_{\text{arom}}$  peak. The BE of the  $C_{\text{CO}}$  peak is 286.010 eV and its FWHM is 1.200 eV. The  $C_{\text{O}}$  peak is located to the left of this peak at a BE of 286.723 eV and a FWHM of 1.152 eV.

In contrast to the  $\alpha$ -phase C1s XPS spectra of the monolayer, the multilayer spectrum in Figure 5.3 exhibits a divergent shape.

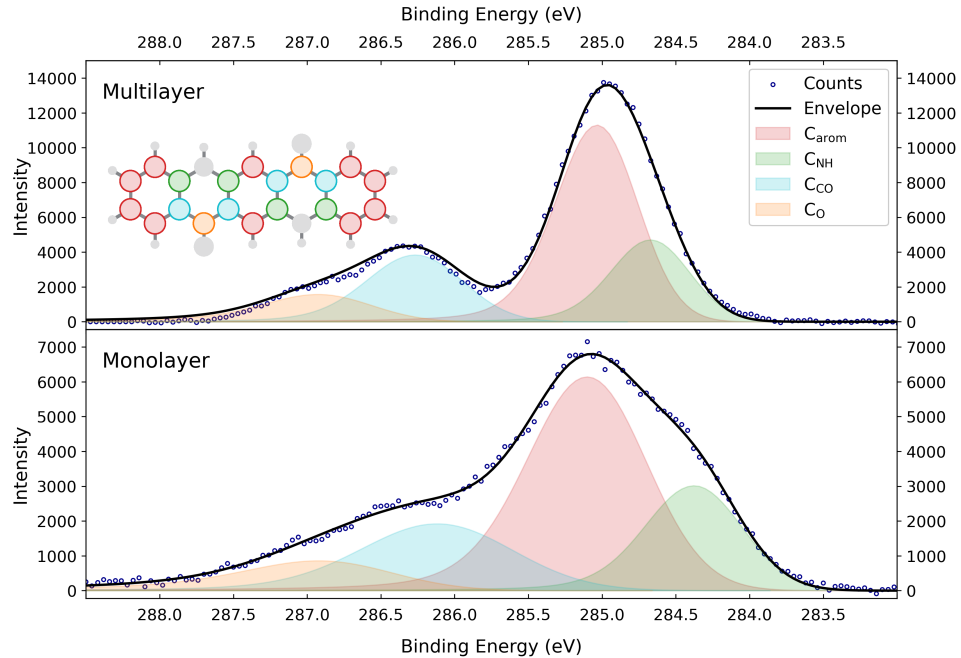


Figure 5.3: C1s XPS spectrum for the  $\alpha$ -phase of QA on Ag(100) for a multilayer coverage compared to the XPS spectrum for a coverage of 1 ML.

Initially, the multilayer spectrum can still be adequately characterized by using the four distinct peaks, which possess equivalent area ratios to those of the monolayer spectrum. However, it is evident that the multilayer spectrum exhibits a significantly heightened intensity relative to the monolayer spectrum. The primary distinctions are evident in the BE and the FWHM of the peaks. The spectrum displays a discernible minimum between the aromatic carbon peak  $C_{\text{arom}}$  and the carbonyl carbon peak  $C_{\text{O}}$ . The peak associated with the amine group ( $C_{\text{NH}}$ ) exhibits a shift towards the  $C_{\text{arom}}$  peak.

### 5.1.2 O1s spectra

Figure 5.4 presents a series of XPS spectra for the O1s photoemission lines of QA at three different coverages: 0.33 ML, 0.79 ML and 1 ML. A prominent peak centered near 531 eV is exhibited by all spectra, a characteristic of the oxygen atoms in carbonyl functional groups present in the QA molecule. Additionally, the shape of the peak suggests the presence of a more intricate structure than a single peak. The spectra exhibit a comparable overall shape and peak position across the various surface coverages.

As anticipated, the spectral intensity increases with coverage, indicative of an increased number of QA molecules adsorbed on the surface. Beyond the intensity changes, differences in peak width and asymmetry are also observed. The spectrum at the lowest coverage (0.33 ML) is narrower and more symmetric, whereas the spectra at higher coverages become progressively broader and more asymmetric.

In summary, the O1s XPS spectra of QA on Ag(100) are qualitatively similar across coverages. A peak assignment and more detailed evaluation will be provided in a subsequent part to elucidate the specific spectral components contributing to the observed features.

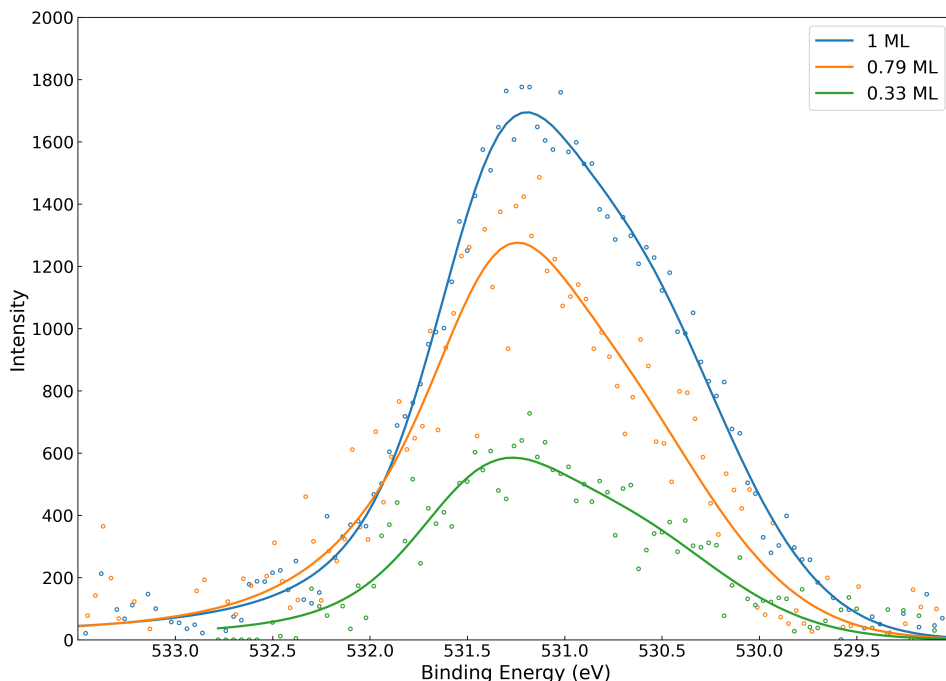


Figure 5.4: Overview of O1s XPS spectra for all preparation of the  $\alpha$ -phase of QA on Ag(100)

A detailed O1s spectrum of QA on Ag(100) at a 1 ML coverage reveals two distinguishable spectral components, which is shown in Figure 5.5.

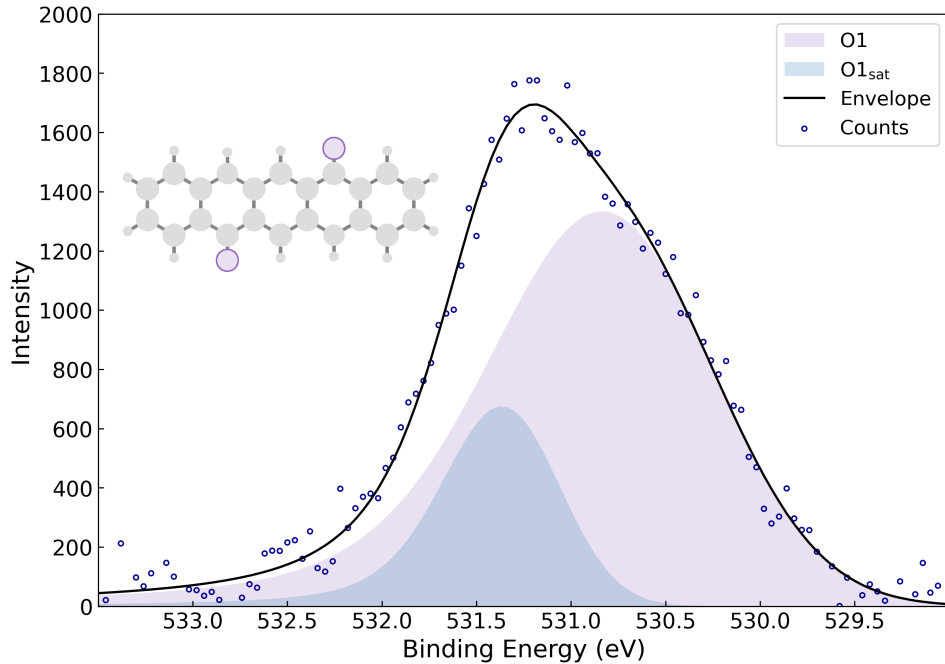


Figure 5.5: O1s XPS spectrum for the  $\alpha$ -phase of QA on Ag(100) for a coverage of 1 ML.

As illustrated in Figure 5.5 and Table 5.2, the primary component (O1) is at a BE of 530.657 eV, exhibiting a FWHM of 1.360 eV. This peak is attributed to the core-level photoemission from oxygen atoms situated within carbonyl functionalities. The relatively broad linewidth is indicative of slight variations in the local chemical environment of these oxygen atoms.

A secondary, less intense component (O1<sub>sat</sub>) is observed at a higher BE of 531.273 eV with a narrower FWHM of 0.712 eV. This feature is interpreted as a shake-up satellite, arising from e.g. a  $\pi - \pi^*$  transition within the conjugated  $\pi$  system of the QA molecule.

Quantitative analysis of the peak areas reveals that the satellite-to-main peak area ratio is approximately 0.27, which is equivalent to 21 % of the total O1s intensity. This ratio is consistent with the expected intensity of shake-up features in aromatic systems with significant conjugation.<sup>[40]</sup>

The combination of these two components provides a comprehensive representation of the O1s photoemission lines of QA. This representation reflects both the intrinsic chemical identity of the oxygen atoms and the dynamic electron processes that accompany core-level photoemission.

Table 5.2: Fit parameter used in CasaXPS<sup>[39]</sup> for the  $\alpha$ -phase of QA on Ag(100) for the O1s photoemission lines..

peak	BE / eV	area ratio	FWHM / eV
O1	530.657	2.00	1.360
O1 <sub>sat</sub>	531.273	0.53	0.712

In Figure 5.6, a XPS spectrum with a multilayer coverage is compared to the previously discussed XPS spectrum.

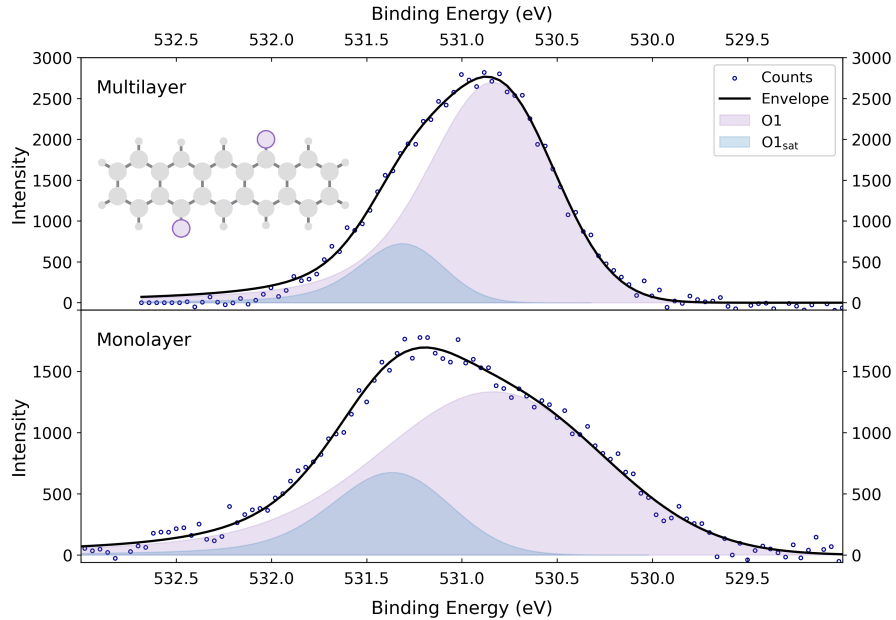


Figure 5.6: O1s XPS spectrum for the  $\alpha$ -phase of QA on Ag(100) for a multilayer coverage compared to the XPS spectrum for a coverage of 1 ML.

The O1s XPS spectrum recorded for QA on Ag(100) at multilayer coverage reveals a well-defined structure characterized by two distinct photoemission peaks. The primary component (O1) is at a BE of 530.733 eV and a FWHM of 0.75 eV. In comparison with the ML O1 peak, the peak position undergoes a change of approximately 0.076 eV. A more salient finding is the change in the FWHM of approximately 0.61 eV, which nearly corresponds to a 50 % alteration.

The satellite peak (O1<sub>sat</sub>) is observed at 531.24 eV with a FWHM of 0.5 eV. Once more, the position of the O1<sub>sat</sub> peak in relation to the ML remains constant. However, the FWHM of the peak decreases by 0.21 eV, which corresponds to approximately 30 %. This alteration may be attributable to the enhanced intensity exhibited by the multilayer XPS spectrum. The satellite-to-main ratio experiences a decrease from 0.27 in the ML to 0.18 in the multilayer, indicating a reduced shake-up process.



### 5.1.3 N1s spectra

The XPS spectra displayed in Figure 5.7 show the N1s photoemission lines of QA on Ag(100) with varying coverages between 0.26 ML and 1 ML. A prominent main peak centered around 400 eV is exhibited by all spectra. Despite the general spectral similarities across different coverages, clear distinctions emerge in the shape and intensity of the main peak. As the coverage increases from submonolayer to monolayer, the main peak systematically increases in intensity, reflecting the proportional increase in nitrogen-containing molecules. In scenarios where coverages are less substantial, the spectra tend to manifest as marginally broader. Conversely, as the coverage increases, the spectra become more narrow.

Additionally, a secondary peak is evident on the low-BE side of the main peak in some spectra at approximately 398 eV. In summary, while the core features of the XPS of QA remain largely preserved across different coverages, changes are observed in peak intensity and width, in addition to the second peak at a lower BE.

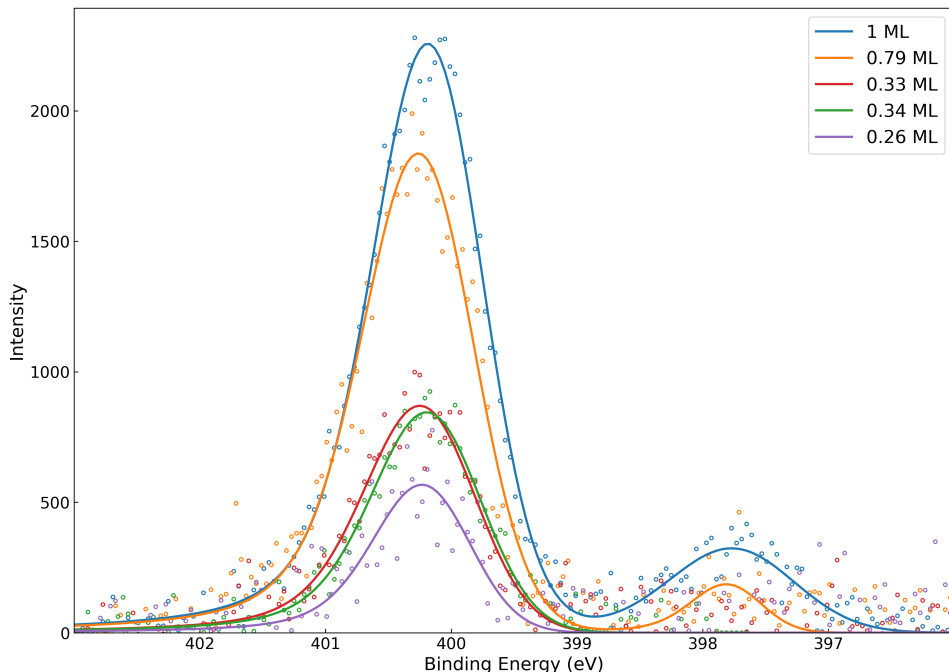


Figure 5.7: Overview of N1s XPS spectra for all preparation of the  $\alpha$ -phase of QA on Ag(100)

The N1s XPS spectrum of QA on Ag(100) with a coverage of 1 ML, as depicted in Figure 5.7, is discussed in more detail in Figure 5.8, which presents the different peaks.

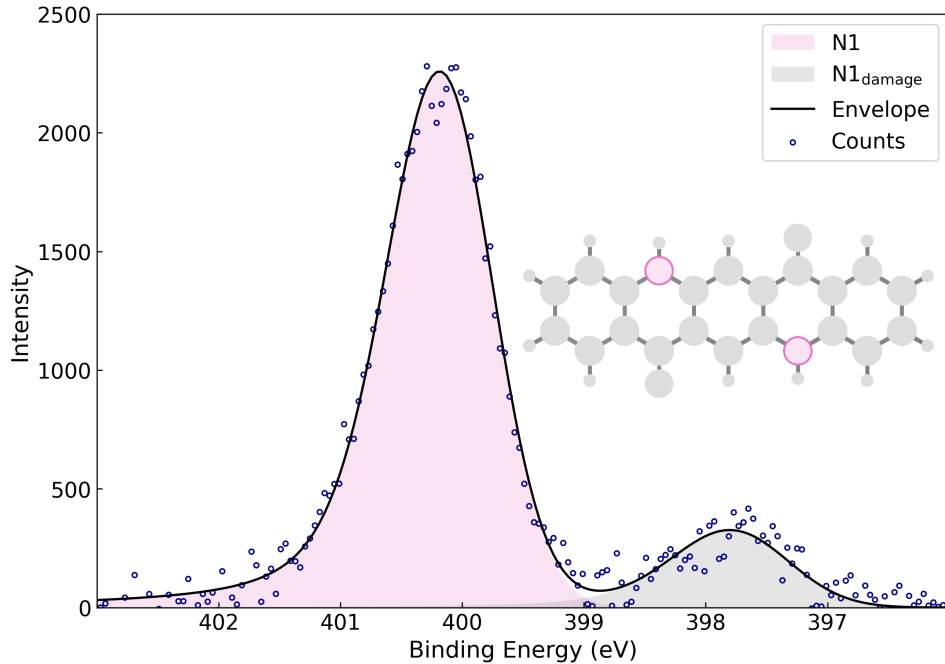


Figure 5.8: N1s XPS spectrum for the  $\alpha$ -phase of QA on Ag(100) for a coverage of 1 ML.

The XPS spectrum in Figure 5.8 can be divided into two discrete components: a primary peak (N1) and a secondary feature at lower BE (N1<sub>damage</sub>). The precise values for the two peaks are enumerated in Table 5.3. The N1 peak, with a center at 400.054 eV and a FWHM of 1.01406 eV, is attributed to nitrogen atoms embedded within the chemically intact QA molecule. The narrow FWHM and symmetrical peak profile are indicative of a well-defined and electronically homogenous nitrogen environment.

The secondary component, N1<sub>damage</sub>, emerges at a BE of 397.656 eV and exhibits a FWHM of 1.12 eV,. This phenomenon is attributed to the presence of chemically modified nitrogen species, which are most likely the result of radiation-induced damage due to prolonged X-ray exposure.

A thorough qualitative analysis was conducted, which yielded a damage-intensity-ratio of 0.16. This ratio indicated that the majority of nitrogen atoms maintain their molecular integrity under the measurement conditions, while a minor but significant portion experiences beam damage.

Table 5.3: Fit parameter used in CasaXPS<sup>[39]</sup> for the  $\alpha$ -phase of QA on Ag(100) for the N1s photoemission lines.

peak	BE / eV	area ratio	FWHM / eV
N1	400.054	2.00	1.017
N1 <sub>damage</sub>	397.656	0.31	1.160

A comparison of the N1s XPS spectrum of the monolayer and the spectrum corresponding to the multilayer is illustrated in Figure 5.9.

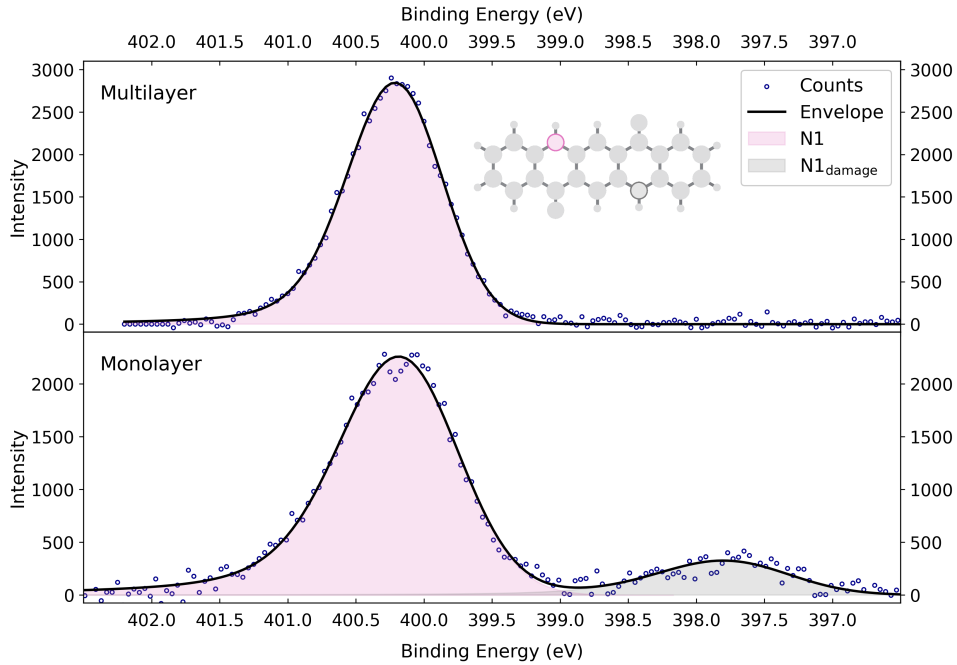


Figure 5.9: N1s XPS spectrum for the  $\alpha$ -phase of QA on Ag(100) for a multilayer coverage compared to the XPS spectrum for a coverage of 1 ML.

The XPS spectrum with a multilayer coverage reveals a single component (N1 centered at a BE of 400.147 eV, accompanied by a FWHM of 0.82 eV. This observation signifies a subtle modification in the chemical environment surrounding the nitrogen atom. The peak associated with beam damage (N1<sub>damage</sub>) remains undetected. This absence indicated that the spectrum of the multilayer originated predominantly from chemically intact nitrogen species. The BE exhibits a slight increase (0.93 eV) in the multilayer, accompanied by a narrower FWHM.



## 5.2 C1s XPS spectra for the phase transition

The Figure 5.10 illustrates C1s photoemission lines for QA molecules absorbed on an Ag(100) substrate, showing the transition from the  $\alpha$ - to the  $\beta$ -phase. The XPS spectra are arranged vertically, with the  $\alpha$ -phase shown at the top, the  $\beta$ -phase at the bottom and a series of intermediate XPS spectra representing the thermally induced phase transition. Maximum values for each individual peak are denoted by a colored vertical line. The phase transition occurs at a temperature of 450 K, which was the target temperature during the recording of the XPS spectra.

In the  $\alpha$ -phase, the C1s XPS spectrum is characterized by distinct peaks corresponding to various chemically different carbon atoms, including the  $C_{\text{arom}}$ ,  $C_{\text{NH}}$ ,  $C_{\text{CO}}$  and  $C_{\text{O}}$  peaks, as discussed in subsection 5.1.1. In the final  $\beta$ -phase, the C1s XPS spectrum demonstrates altered peak intensities and BEs in comparison to the initial  $\alpha$ -phase. It is noteworthy that all peaks undergo modification, which is indicative of a thermally induced structural rearrangement or reorientation of the QA molecule. The sequence demonstrates a substantial trend for all peaks. A systematic, stepwise decrease in BEs is exhibited by all four peaks. A comparative analysis of the  $C_{\text{arom}}$ ,  $C_{\text{CO}}$  and  $C_{\text{O}}$  peaks reveals a consistent pattern of change.

A further difference in the change is observed in the  $C_{\text{NH}}$  peak. The shifts towards lower BEs is less pronounced in comparison to the other peaks. This indicates that the environments of the other C1s photoemission lines, namely  $C_{\text{arom}}$ ,  $C_{\text{CO}}$  and  $C_{\text{O}}$ , are changed in a similar way, while the  $C_{\text{NH}}$  carbon atoms experiences a different change in its chemical surrounding.

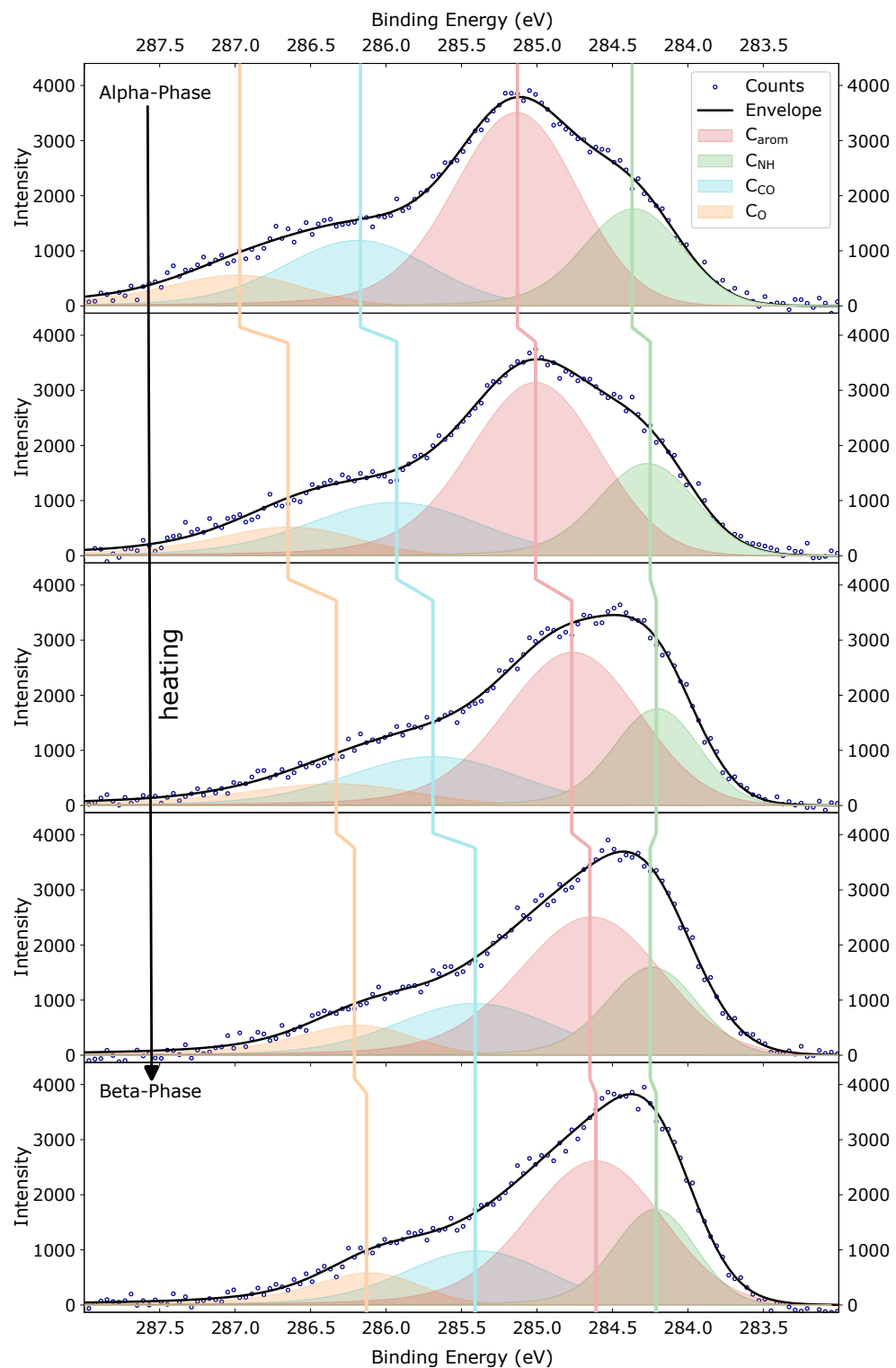


Figure 5.10: C1s XPS spectrum for the phase transition from the  $\alpha$ - to the  $\beta$ -phase of QA on Ag(100).

## 5.3 The commensurate 2D $\beta$ -Phase

The ensuing discourse will examine the phase designated as the  $\beta$ -phase. The investigation of the  $\beta$ -phase was conducted once more on all three available photoemission lines: C1s, O1s, and N1s. To address this need, the present chapter has been meticulously subdivided into discrete sections, each dedicated to specific photoemission lines. A comprehensive analysis of a particular XPS spectrum of the  $\beta$ -phase is presented in each section, along with a comparative analysis of the  $\alpha$ - and  $\beta$ -phases.

### 5.3.1 C1s spectra

The C1s XPS spectrum for the  $\beta$ -phase of QA on Ag(100) is presented in Figure 5.11.

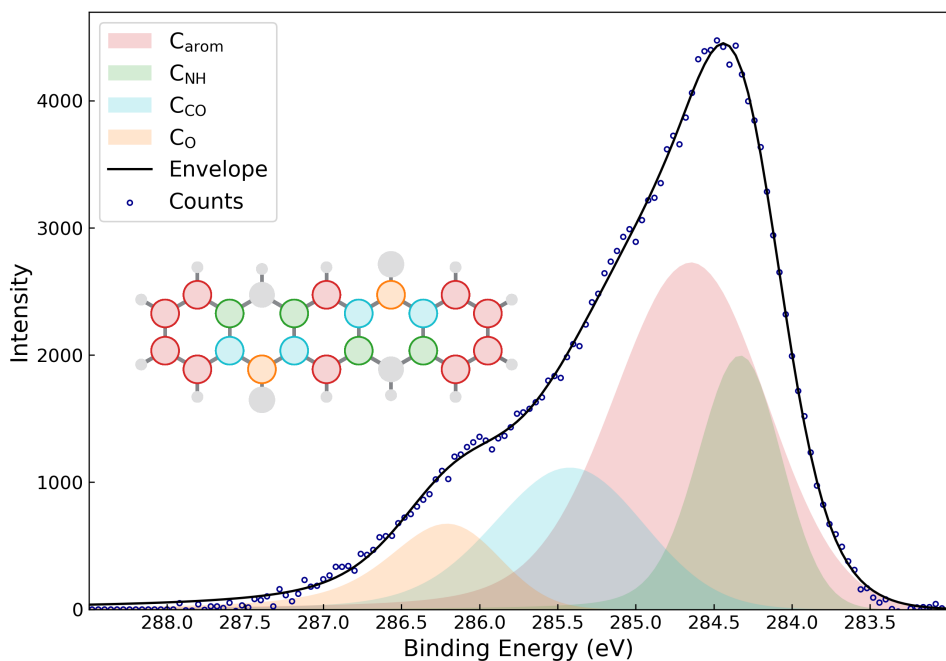


Figure 5.11: C1s XPS spectrum for the  $\beta$ -phase of QA on Ag(100).

The XPS spectrum of QA in the  $\beta$ -phase displays four distinct components, designated as C<sub>arom</sub>, C<sub>NH</sub>, C<sub>CO</sub> and C<sub>O</sub>, which bear the same nomenclature as in the  $\alpha$ -phase. This finding suggests that the various carbon atoms present within the QA molecule exhibit a persistent correlation with distinct peaks in the XPS spectrum.

The primary component, C<sub>arom</sub>, is located at a BE of 284.545 eV with a FWHM of 1.132 eV. The second peak, characterized by a BE of 284.275 eV and a FWHM of 0.618 eV, is identified as the C<sub>NH</sub> peak. The C<sub>CO</sub> peak is located at a BE of 285.322 eV, experiencing a FWHM of 1.107 eV. In the vicinity of this peak, at a higher BE, is the C<sub>O</sub> peak at 286.072 eV with a FWHM of 0.785 eV.

A qualitative investigation of the peak areas yielded analogous results to those of the  $\alpha$ -phase, wherein the area ratios exhibited precise congruence with the number of carbon atoms in the QA molecule.

In summary, the XPS spectrum for C1s components of the  $\beta$ -phase offers significant insights into the chemical changes that occur between the  $\alpha$ - and  $\beta$ -phase. The single peaks are compared to each other, thereby providing information about the local environment around the carbon atoms.

Table 5.4: Fit model of the  $\beta$ -phase for C1s.

peak	BE / eV	area ratio	FWHM / eV
C <sub>arom</sub>	284.545	10	1.132
C <sub>NH</sub>	284.275	4	0.618
C <sub>CO</sub>	285.322	4	1.107
C <sub>O</sub>	286.072	2	0.785

In order to facilitate a more robust comparison of the  $\beta$ -phase to the  $\alpha$ -phase, the C1s XPS spectra of these two phases are presented in Figure 5.12.

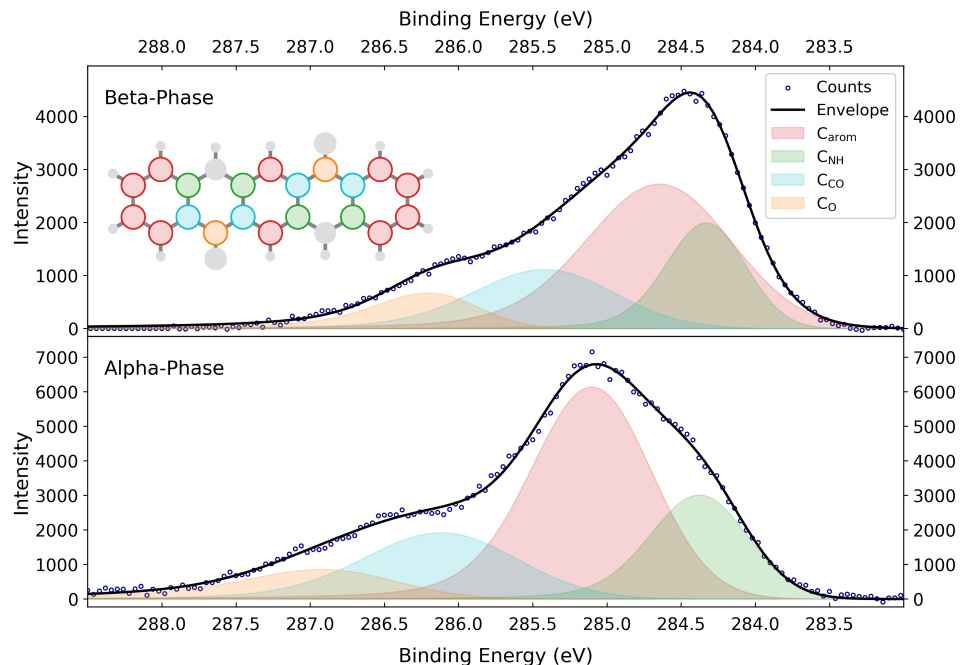


Figure 5.12: C1s XPS spectrum for the  $\alpha$ - and  $\beta$ -phase of QA on Ag(100).

A close examination reveals that all four peaks shift to a lower BE. The shift in the BE of the C<sub>NH</sub> peak is, by far, the least significant. The three other peaks, C<sub>arom</sub>, C<sub>CO</sub> and C<sub>O</sub>, demonstrate a comparable shift in the BE.

A further noteworthy discrepancy is the increase of the FWHM for the C<sub>arom</sub> peak, which is approximately 0.19 eV. The three other peaks demonstrate a decrease in their FWHM. It is remarkable that the FWHM of the C<sub>O</sub> peak decreases by 0.37 eV. The observed variation could be attributed to the underlying interconnectedness of all four peaks, which demonstrate a certain degree of interdependence.

In summary, the alterations in BEs and FWHM values of the four peaks result in a significantly divergent XPS spectrum. Consequently, QA on Ag(100) in the  $\beta$ -phase is expected to demonstrate a comparable significant change compared to the  $\alpha$ -phase.



### 5.3.2 O1s spectra

As illustrated in Figure 5.13, the XPS spectrum for the O1s components for the  $\beta$ -phase of QA on Ag(100) is presented.

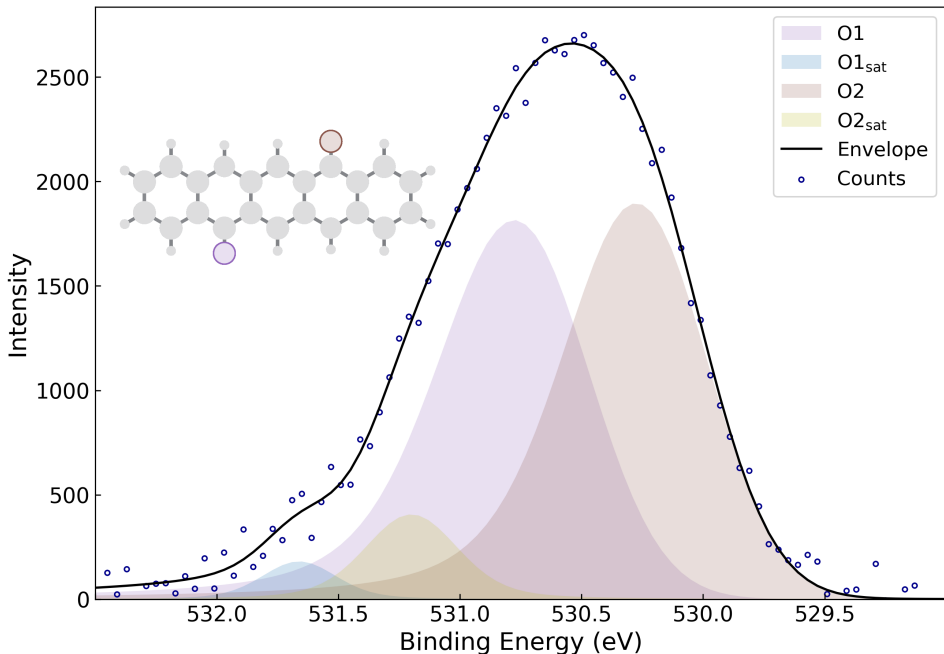


Figure 5.13: O1s XPS spectrum for the  $\beta$ -phase of QA on Ag(100).

The XPS spectrum of the  $\beta$ -phase in Figure 5.13 consists of two peaks, each with its own satellite. The detailed data of the overall four peaks are shown in Table 5.5. The O1 peak is located at a BE of 530.683 eV with a FWHM of 0.712 eV. The respective satellite is at 531.661 eV with a FWHM of 0.362 eV. This corresponds to a shift in BE of 0.978 eV.

The other peak, O2, has a slightly lower BE of 530.186 eV but a similar FWHM of 0.681 eV. The satellite O2<sub>sat</sub> also has a similar shift of 1.014 eV and is located at a BE of 531.200 eV with a FWHM of 0.451 eV. The O1 and O2 have an area ratio of 1:1, which corresponds to one oxygen atom for each peak.

In summary, the FWHM of two peaks are around 0.7 eV and both have a shake-up satellite with a higher BE by approximately 1.0 eV. The two peaks are 0.5 eV apart from each other.

Table 5.5: Fit model of the  $\beta$ -phase for O1s.

peak	BE / eV	area ratio	FWHM / eV
O1	530.683	1	0.712
O1 <sub>sat</sub>	531.661	0.05	0.362
O2	530.186	1	0.681
O2 <sub>sat</sub>	531.200	0.14	0.451

To enable a better comparison between  $\alpha$ - and  $\beta$ -phase, both spectra are depicted in Figure 5.14.

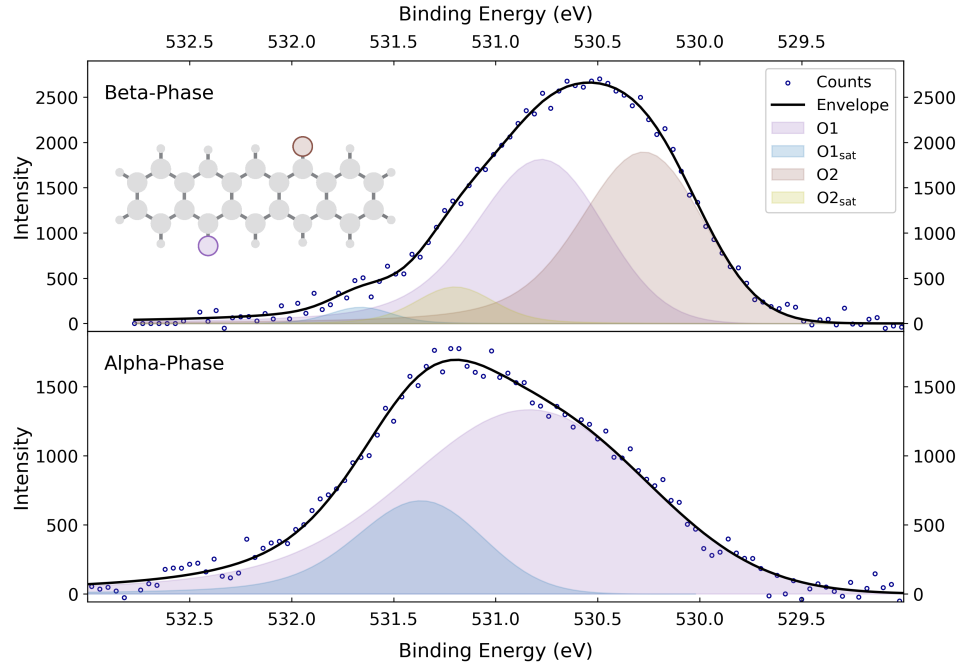


Figure 5.14: O1s XPS spectrum for the  $\alpha$ - and  $\beta$ -phase of QA on Ag(100).

The investigation of the differences between the two phases yields that the O1 peak does not change its position but exhibits a change in its FWHM towards a smaller value. Same holds true for the O1<sub>sat</sub> peak, which also changes its BE by approximately 0.4 eV.

The most significant change is obviously the second peak, occurring at the  $\beta$ -phase. This means that the two chemically equivalent peaks from the  $\alpha$ -phase have changed their environment, leading to two chemically different oxygen atoms in the  $\beta$ -phase.

### 5.3.3 N1s spectra

As depicted in Figure 5.15, the N1s XPS spectrum for the  $\beta$ -phase of QA on Ag(100) has been presented.

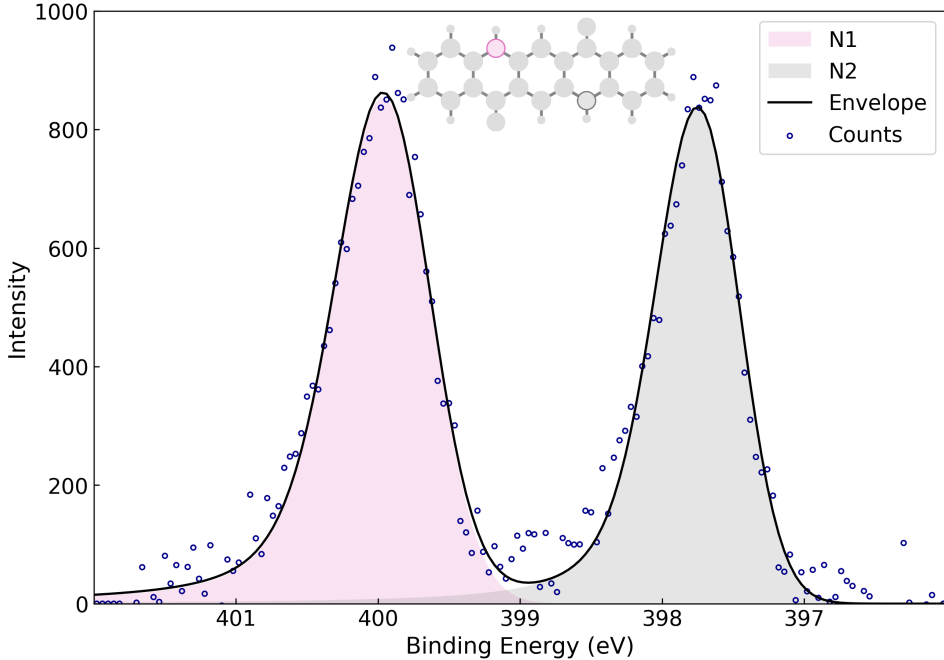


Figure 5.15: N1s XPS spectrum for the  $\beta$ -phase of QA on Ag(100).

Figure 5.15 and Table 5.6 enable a quantitative description of the N1s XPS spectrum for the  $\beta$ -phase. As seen, the  $\beta$ -phase has two different peaks for N1s, namely N1 and N2. Both peaks have a similar FWHM of 0.774 eV and 0.686 eV. Furthermore, they have the same intensity and an area-ratio of 1:1. This indicates that each peak corresponds to one of the nitrogen atoms of QA.

The main difference of the two peaks is their BE. The N1 peak is located at a BE of 399.865 eV while the N2 peak has a BE of 397.661 eV. This means that the peaks are separated by 2.20 eV. In comparison to the shifts in BEs for the other photoemission lines, this value seems to indicate a quite drastic change in the chemical environment of one of the nitrogen atoms.

Table 5.6: Fit model of the  $\beta$ -phase for N1s.

peak	BE / eV	area ratio	FWHM / eV
N1	399.865	1	0.774
N2	397.661	1	0.686

To enable a comparative analysis between the  $\alpha$ - and the  $\beta$ -phase, the two phases are depicted in a juxtaposed arrangement in Figure 5.16.

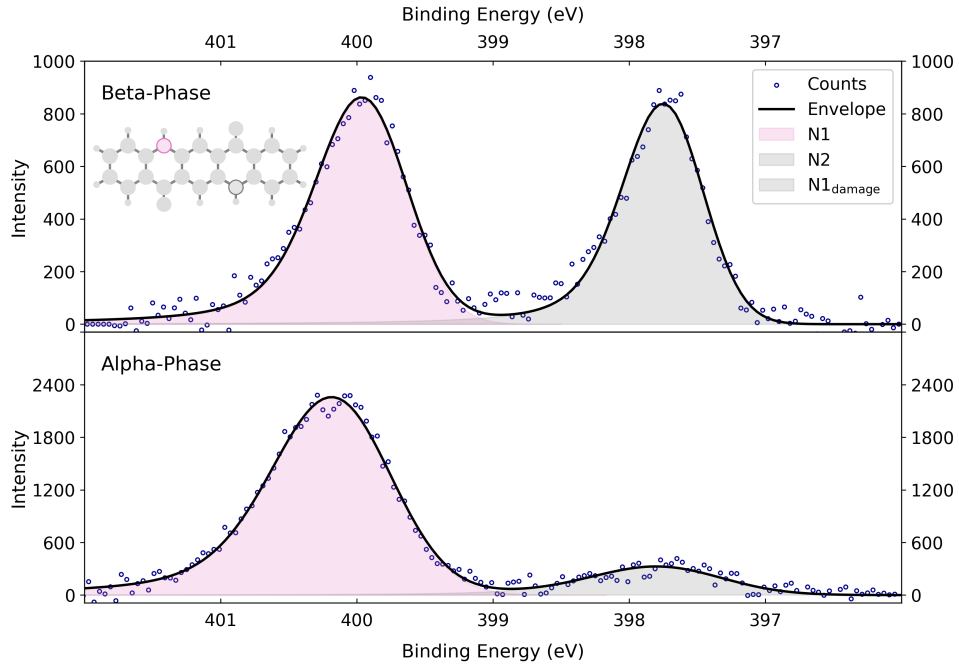


Figure 5.16: N1s XPS spectrum for the  $\alpha$ - and  $\beta$ -phase of QA on Ag(100).

The comparison of the  $\alpha$ - and the  $\beta$ -phase yields interesting results about the nitrogen atoms. First, the N1 peak keeps almost the same BE in both phases. There is only a change in BE of about 0.188 eV towards a lower value. The more significant change can be observed in the change of the FWHM, decreasing from 1.017 eV to 0.774 eV. This corresponds to a sharper peak in the XPS spectrum, indicating a more homogenous environment for the N1 peak.

Nevertheless, the other peak, namely N2, reveals a more intriguing finding, prompting further examination. The N2 peak has exactly the same BE as the N1<sub>damage</sub> peak of the  $\alpha$ -phase. As seen in Figure 5.16, the areas of the N2 peak in the different phases can not be compared anyhow, which also makes an comparison of the FWHM unsuitable.

## 5.4 Binding energy changes upon phase transition

For a further comparison of the differences in the BEs between the  $\alpha$ - and the  $\beta$ -phase, an overview of these are illustrated in Figure 5.17.

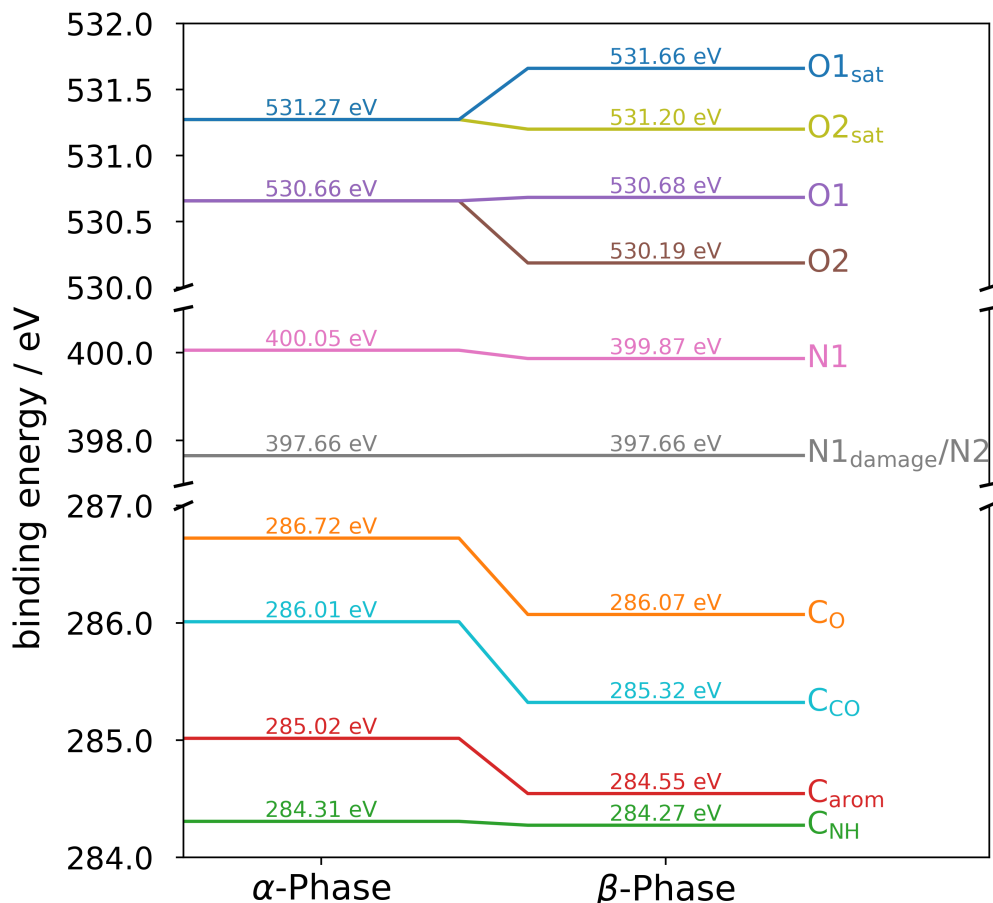


Figure 5.17: Illustration of the shift in the BE from the  $\alpha$ - to the  $\beta$ -phase of QA on Ag(100) for the different peaks in the XPS spectra for all core-levels.

Initially, a significant trend is observed in all peaks across all XPS spectra. The BEs of all atoms in the  $\beta$ -phase are lower than or similar to those of the atoms in the  $\alpha$ -phase.

Starting with the XPS spectra for C1s, the differences in the BEs are subsequently examined in detail. Shifts in the BE for three of the four peaks, namely  $C_{\text{arom}}$ ,  $C_{CO}$  and  $C_O$  are similar. They all decrease by 0.5-0.7 eV. Conversely, the BE of the  $C_{NH}$  peak does not significantly decrease. This indicates that the carbon atoms next to the amine undergo a different change during phase transition than the other carbon atoms.

Consequently, the XPS spectra for N1s are of great interest. As previously mentioned, the  $\beta$ -phase exhibits two peaks instead of one for N1s. The second peak in the  $\beta$ -phase is more than 2 eV lower in BE than the first peak. This represents a significant difference in the BE that is not observed for any other peak. To provide an example, the BE difference between the C<sub>NH</sub> and the C<sub>O</sub> peak, despite their very different chemical environments, is only 1.8 eV.

Lastly, the BEs of the two phases for the O1s XPS spectra are compared. Again, there are two distinct peaks in the  $\beta$ -phase instead of one in the  $\alpha$ -phase. The BE of one peak remains at roughly the same value, while the other decreases by about 0.4 eV. This result is similar to the change in BE observed in the C1s XPS spectra.

# 6 Discussion

The  $\alpha$  and  $\beta$ -phase of QA on Ag(100) were investigated using XPS for three different components: C1s, O1s and N1s. The ensuing discourse will meticulously examine the results obtained from chapter 5, which will be methodically organized into discrete chapters to facilitate a comprehensive analysis of each phase.

## 6.1 The 1D $\alpha$ -Phase

The C1s XPS spectra consist of four distinct components, corresponding to distinct carbon atoms in the QA molecule, namely  $C_{\text{arom}}$ ,  $C_{\text{NH}}$ ,  $C_{\text{CO}}$  and  $C_{\text{O}}$ .

The carbon atoms  $C_{\text{arom}}$  have the least influence from the functional groups. This leads to a BE in the center of the spectrum. Due to the number of carbon atoms associated with this peak, the peak area is the most substantial, and the peak provides the primary contribution to the overall shape of the spectrum. The BE of the peak appears to be realistic, as evidenced by its alignment with other molecular adsorbed on Ag(100), such as perylenetetracarboxylic dianhydride (PTCDA), which exhibit comparable values.<sup>[40]</sup>

The peak corresponding to the carbon atoms adjacent to the amine, designated as  $C_{\text{NH}}$ , is located at a slightly decreased BE in comparison to the  $C_{\text{arom}}$  peak. This behavior of aromatic systems with amine functional groups inside, such as those found in pyridine, is typically observed.<sup>[41,42]</sup>

The peak that arises due to beam damage ( $N1_{\text{damage}}$ ) has a shift in its BE of around 2.20 eV. This large difference indicates a drastic change in the chemical environment of the nitrogen atom. Compared to other shifts in the BE, e.g. for the carbon atoms, the influence of other neighboring atoms are not enough to explain this change. For this reason, something different has to happen at the nitrogen atom due to beam damage.

A typical observed phenomena for the amine group is the deprotonation of the nitrogen atom. The deprotonation of amine groups in XPS spectra was examined with a shift in the BE of about 2-3 eV.<sup>[43,44]</sup> This matches to the results found for the  $N1_{\text{damage}}$  peak, leading to the assumption that the x-ray beam deprotonates some of the nitrogen atom .

Last, the XPS spectra for the O1s components are discussed. The BE of the O1 peak matches to similar systems, e.g. PTCDA on Ag(100).<sup>[40]</sup> The satellite peak,  $O1_{\text{sat}}$ , observed for QA was also measured for PTCDA. The satellite peaks for the two adsorbates have similar shifts in their BEs and area ratios. This indicates that the results of the O1s XPS spectra and the fit model is realistic.

In summary, the entirety of the peaks in the XPS spectra adequately describe the molecular structure of QA and are in accordance with the literature. In addition, the observed peaks in the XPS spectra corroborate the structure model proposed by N. Humberg.<sup>[10]</sup> The chemical environment of all nitrogen and oxygen atoms is identical within the structure model, because all oxygen atoms of one molecule form a hydrogen bond with the amine group of another molecule. This is evident from the XPS spectra, which exhibit only a single peak for the corresponding atoms. Furthermore, the results indicates that all molecules in the structure have a similar chemical environment, which also matches to the structure model.

## 6.2 Phase transition

The examination of the phase transition was made with measuring a sequence of C1s XPS spectra while increasing the sample temperature. This sequence shows in principle that the phase transition from the  $\alpha$ - to the  $\beta$ -phase occurs in a stepwise manner while heating the sample to 450 K. A close examination of the data reveals a transition in each peak from one spectrum to the next XPS spectrum. This indicates that all molecules would undergo simultaneous and analogous changes.

While this assumption may be theoretically valid, it appears to be improbable. A more probable theory posits that the phase occurs for some molecules prior to others, resulting in a decreases of the  $\alpha$ -phase and an increase the  $\beta$ -phase. This observation aligns with the findings reported by N. Humberg.<sup>[10]</sup> Nevertheless, the exact process of the phase transition can not be verified with the given data.

## 6.3 The commensurate 2D $\beta$ -Phase

For the  $\beta$ -phase of QA on Ag(100) one set of XPS spectra for all photoemission lines were recorded. First, the C1s XPS spectra are discussed. The  $\beta$ -phase exhibits four distinct peaks, that correspond to the same carbon atoms as in the  $\alpha$ -phase. The relative position, with the C<sub>arom</sub> in the center, the C<sub>NH</sub> peak towards lower, the C<sub>CO</sub> and the C<sub>O</sub> peak towards higher BEs. The three peaks, C<sub>arom</sub>, C<sub>CO</sub> and C<sub>O</sub>, have a similar shift in their BEs. This corresponds to similar changes in their chemical environment.

The lower BE could be explained with stronger interactions between the Ag(100) surface and QA. Thereby, the metal surface could donate electron density to the molecule, resulting in lower BEs. This process is also observed in literature and thus a valid explanation for the observed change in the BE.<sup>[29]</sup>

However, the change exhibited in the C<sub>NH</sub> peak is distinct. The BE remains constant during the phase transition; nevertheless, this phenomenon should not be interpreted in such a simplistic manner. Instead, it should be interpreted as a similar change in the BE towards lower values due to a stronger interaction with the surface and then another effect that increases the BE again. This process involves a change in the nitrogen atom bound to the C<sub>NH</sub> atom. The bond between the carbon and nitrogen

atoms has a significant impact on the electron density at the C<sub>NH</sub> atom and could decrease the electron density. This decreased electron density results in an increase in the BE of the carbon atom.

This leads to the subsequent discussion of the N1s XPS spectra for the  $\beta$ -phase, where the one peak for both nitrogen atoms from the  $\alpha$ -phase divides into two different peaks. At the outset, the BE of the N1 peak undergoes a slight decrease in association with the phase transition. This decrease is less significant than that observed for the other atoms. This implies that the nitrogen atom, corresponding to the N1 peak, exhibits a marginal increase in electron density, while the overall changes are analogous to those observed in the entire molecule. The observed increase in electron density may be attributed to enhanced interactions between the Ag(100) surface and QA.

The second peak for the  $\beta$ -phase is precisely coincident with the position of the peak from the  $\alpha$ -phase, which corresponds to beam damage. It can be posited that the nitrogen atom corresponding to the N2 peak has the equivalent chemical environment as the N1<sub>damage</sub> peak. As previously stated, the N1<sub>damage</sub> peak corresponds to a deprotonated nitrogen atom, a finding that aligns with the literature.<sup>[43,44]</sup> This observation suggests the hypothesis that the observed N2 peak corresponds to a deprotonated nitrogen atom as well.

This means that in each QA molecule exactly one of the two amine groups is deprotonated due to the phase transition. The energy, needed for the deprotonation, has to be overcompensated by the different orientation and stronger interaction with the Ag(100) surface in the  $\beta$ -phase, because the  $\beta$  is thermodynamically favored.<sup>[10]</sup> It is conceivable that the deprotonated nitrogen bonds to the Ag(100) surface and donates electron density to the metal, which would lead to a stabilization of the phase. This process could then overcompensate the energy loss due to deprotonation.

The transition observed from a single peak in the  $\alpha$ -phase to two peaks in the  $\beta$ -phase was likewise detected in the O1s XPS spectra. The BE of the O1 peak remains nearly constant. This phenomena is analogous to that observed for the nitrogen atoms. Consequently, it can be deduced that the nitrogen N1 and the oxygen O1 are the two atoms that interact with each other in the  $\alpha$ - and  $\beta$ -phase. These two atoms still have a hydrogen bond in the  $\beta$ -phase between the keto and the amine group, which leads to similar BEs for both phases.

The second peak in the O1s XPS spectrum for the  $\beta$ -phase then corresponds to the other oxygen atom that interacts with the N2 peak. This O2 peak exhibits a lower BE in comparison to the O1 peak by 0.5 eV. This corresponds to an increased electron density at the oxygen atom, which could be result of a missing hydrogen bond between the oxygen atom from one molecule and the hydrogen atom of an amine group from another molecule.

For the  $\beta$ -phase, both O1s peaks in the XPS spectra have satellites. These are at 1 eV higher BEs than the main peaks, which corresponds to a slight increase in the BE difference between satellite and main peak compared to the  $\alpha$ -phase. This indicates that the shake-up process also changes between the two phases.

The experimental results from the XPS spectra have to be compared to the structure model from N. Humberg.<sup>[10]</sup> First, the structure of the  $\beta$ -phase is commensurate. This

is also seen in the C1s XPS spectra, because it shows precise positions for each of the carbon atoms. Altogether, the C1s XPS spectra match to the structure model of the  $\beta$ -phase.

However, the O1s and N1s XPS spectra contradict the structure model. The XPS spectra show for both atom types two distinct peak with a 1 : 1 area ratio. This observation does not align with the structure model. According to N. Humberg,<sup>[10]</sup> the structure of the  $\beta$ -phase has 1.5 hydrogen bonds per QA molecule, which would correspond to two distinct peaks with an area ratio of 1.5 : 0.5 (3 : 1).

Apart from this, the change in BE for the N1s XPS spectra indicates that 1 of the two nitrogen atoms per molecule is deprotonated. This finding was also not taken into account for the structure model. Furthermore, the deprotonation of one of the two nitrogen atoms would lead to the fact, that 1.5 hydrogen bonds per molecule are not possible anymore.

The results of the experiments lead to a different structure model for the  $\beta$ -phase. Therefore, two theoretically possible structure models are depicted in Figure 6.1, which match to the SPA-LEED image and STM results from N. Humberg.<sup>[10]</sup> The structure models will be discussed in the following.

The first structure model is similar to the one of N. Humberg.<sup>[10]</sup> The positions of the molecules are exactly the same and dimers are also formed. The most important change is the deprotonation of one of the nitrogen atoms per molecule. The most probable nitrogen atom for the deprotonation is the one that is not in between the molecules of the dimer, otherwise there would be no reason to form these dimers. In addition, high electron density at the deprotonated nitrogen atom and at the oxygen atom would repel each other. This results in two hydrogen bonds between the two molecules of the dimer, meaning one hydrogen bond per molecule. No further hydrogen bonds are formed in this structure.

The structure seems the preferred one but there are further aspects that need to be discussed. In model 1, the deprotonated nitrogen, which then has a high electron density, is opposite to the oxygen atom, which also has a high electron density. Usually, the negative charges should repel each other. Nevertheless, it is possible that the nitrogen and the oxygen atom change their height and approach the surface. This could increase the instance between the two atoms. Furthermore, both atoms could donate electron density to the Ag(100) surface, which should also decrease the repulsion.

The second structure model has more changes compared to the one of N. Humberg.<sup>[10]</sup> Instead of the heterochiral dimers, the structure model is homochiral. This means that the molecules do not have to rotate on the surface for the phase transition from the  $\alpha$ - to the  $\beta$ -phase. The model also forms the same amount of hydrogen bridges as model 1.

However, a significant issue has been identified with model 2. As depicted in the structure model, the oxygen atom of one molecule is directly opposite to the oxygen atom of another molecule. The plausibility of this occurrence appears to be minimal, because they should also repel each other. It could also be possible that both oxygen atoms approach the surface and donate electron density to the surface. This could in-

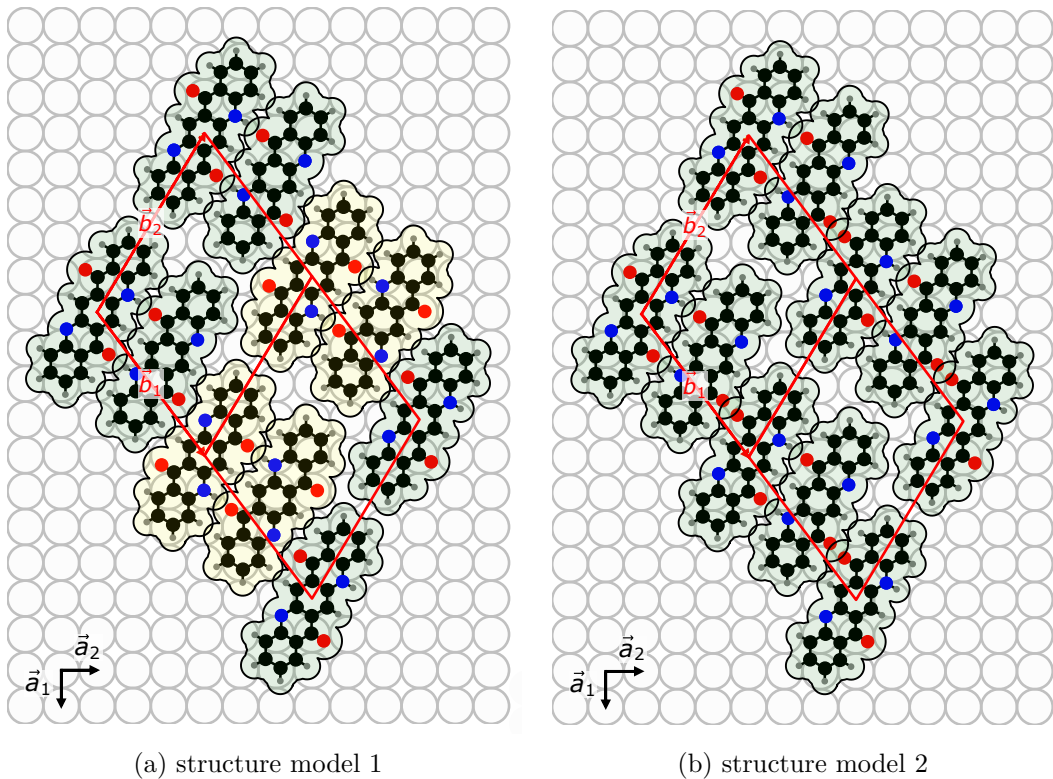


Figure 6.1: Two different structure models for the  $\beta$ -phase of QA on Ag(100).

crease the distance between the atoms and decrease the repulsion. Nevertheless, model 2 appears to be less probable than model 1 for the reasons previously enumerated.



## 7 Summary and Outlook

In summary, the present study has expanded the understanding of the phase behaviour of QA on Ag(100) by examining the  $\alpha$ - and the  $\beta$ -phase in greater detail. The investigation of the  $\alpha$ - and the  $\beta$ -phase was conducted by utilizing XPS for the C1s, N1s and O1s components.

The results for the  $\alpha$ -phase are consistent with the prior findings by N. Humberg.<sup>[10]</sup> The proposed structure model has been confirmed. In addition, all XPS spectra, particularly those of the C1s core-level, can be subdivided into multiple peaks and allocated to particular atoms of QA. Furthermore, the consequences of beam damage due to exposure of QA to the x-ray were investigated. The results demonstrated that the deprotonation of the amine group occurred as a result of this exposure.

A subsequent examination of the results for the  $\beta$ -phase reveals inconsistencies with the proposed structure model by N. Humberg<sup>[10]</sup> for this phase. It was ascertained that the  $\beta$ -phase is composed of two distinct oxygen atoms, exhibiting a stoichiometric ratio of 1 : 1. A comparable observation was made in the case of the nitrogen atoms. Additionally, it was determined that deprotonation of one of the nitrogen atoms is necessary due to its shift in binding energy, leading to only one hydrogen bond per molecule. The findings of this study have led to the proposition of the novel structure model in Figure 6.1.

Nevertheless, the extant structure models leave unresolved questions in need of further investigation. To further refine our comprehension of QA on Ag(100), it is imperative to undertake additional research to develop a more detailed structure model. Therefore, normal incidence x-ray standing wavefield absorption (NIXSW) measurements could be used to determine the adsorption height of the atoms, which allow a revision of the structure model. Beyond that, different NIXSW measurements could be used for triangulation of the  $\beta$ -phase. This should give exact adsorption sites for the atoms and allow a detailed structure model.





## 8 Appendix

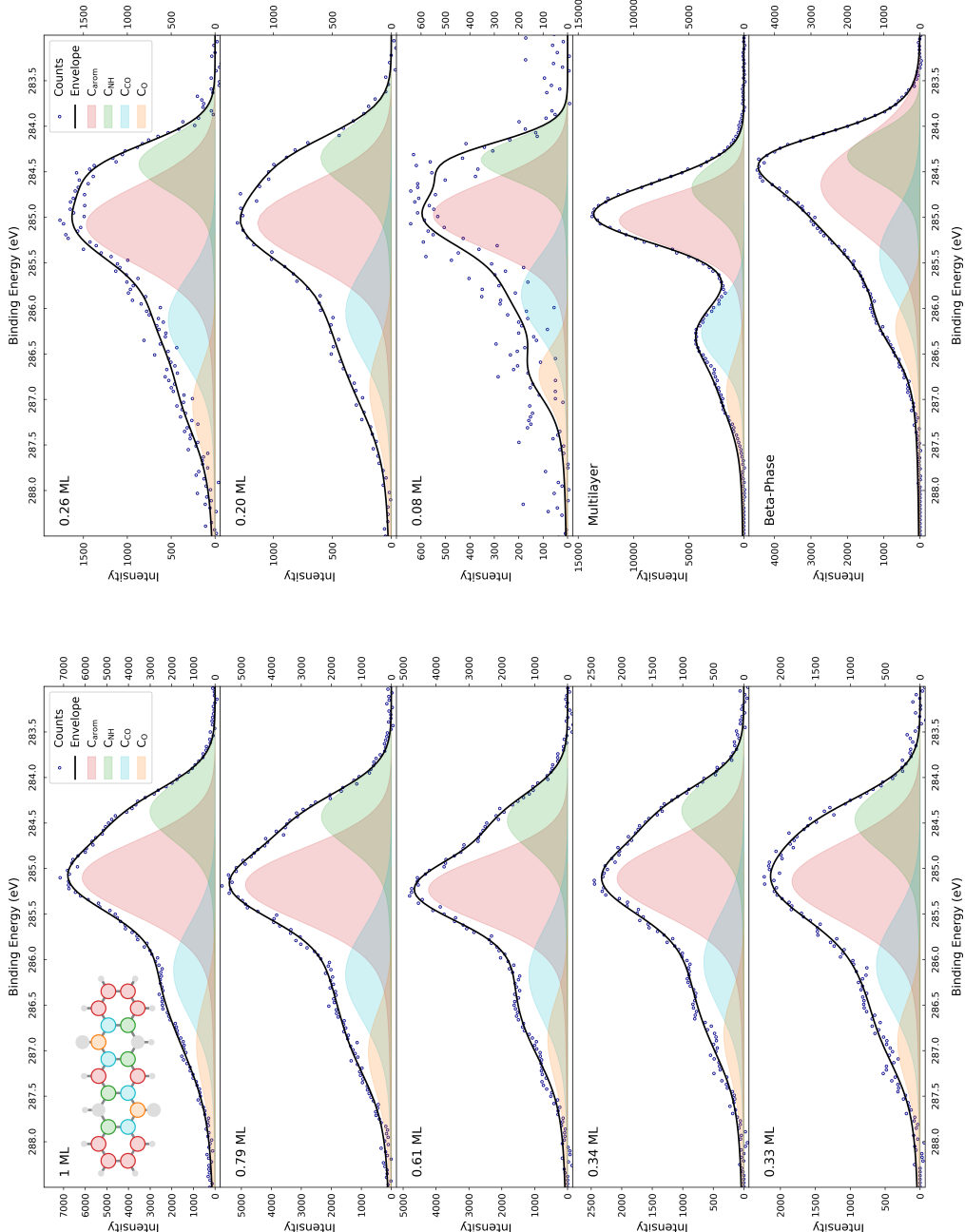


Figure 8.1: Collection of all C1s core-level XPS spectra with the different fitted peaks of all performed experiments. Each spectrum corresponds to a different preparation. The coverage of the first spectrum is set to 1 ML.

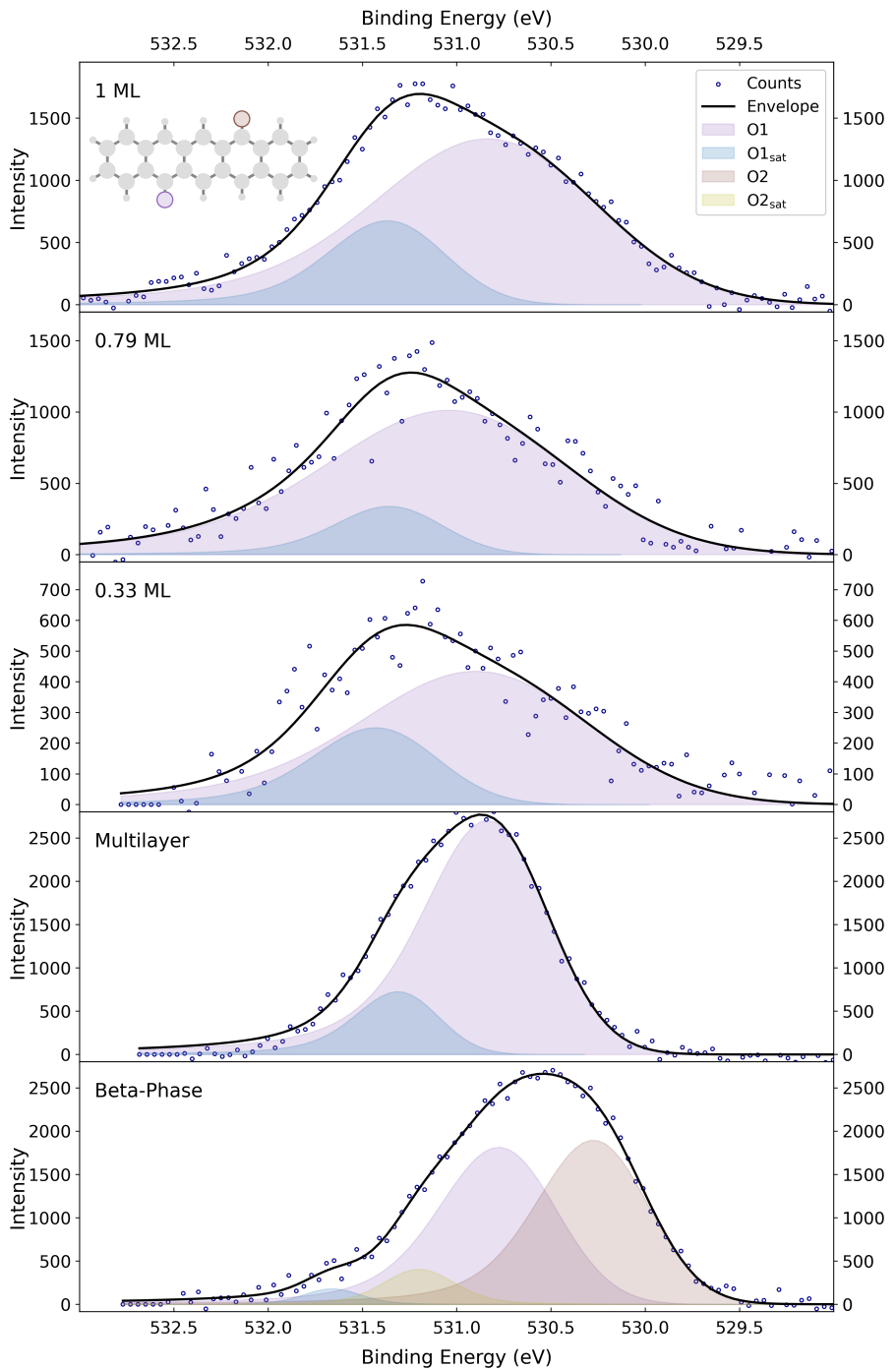


Figure 8.2: Collection of all O<sub>1s</sub> core-level XPS spectra with the different fitted peaks of all performed experiments. Each spectrum corresponds to a different preparation. The coverage of the first spectrum is set to 1 ML.

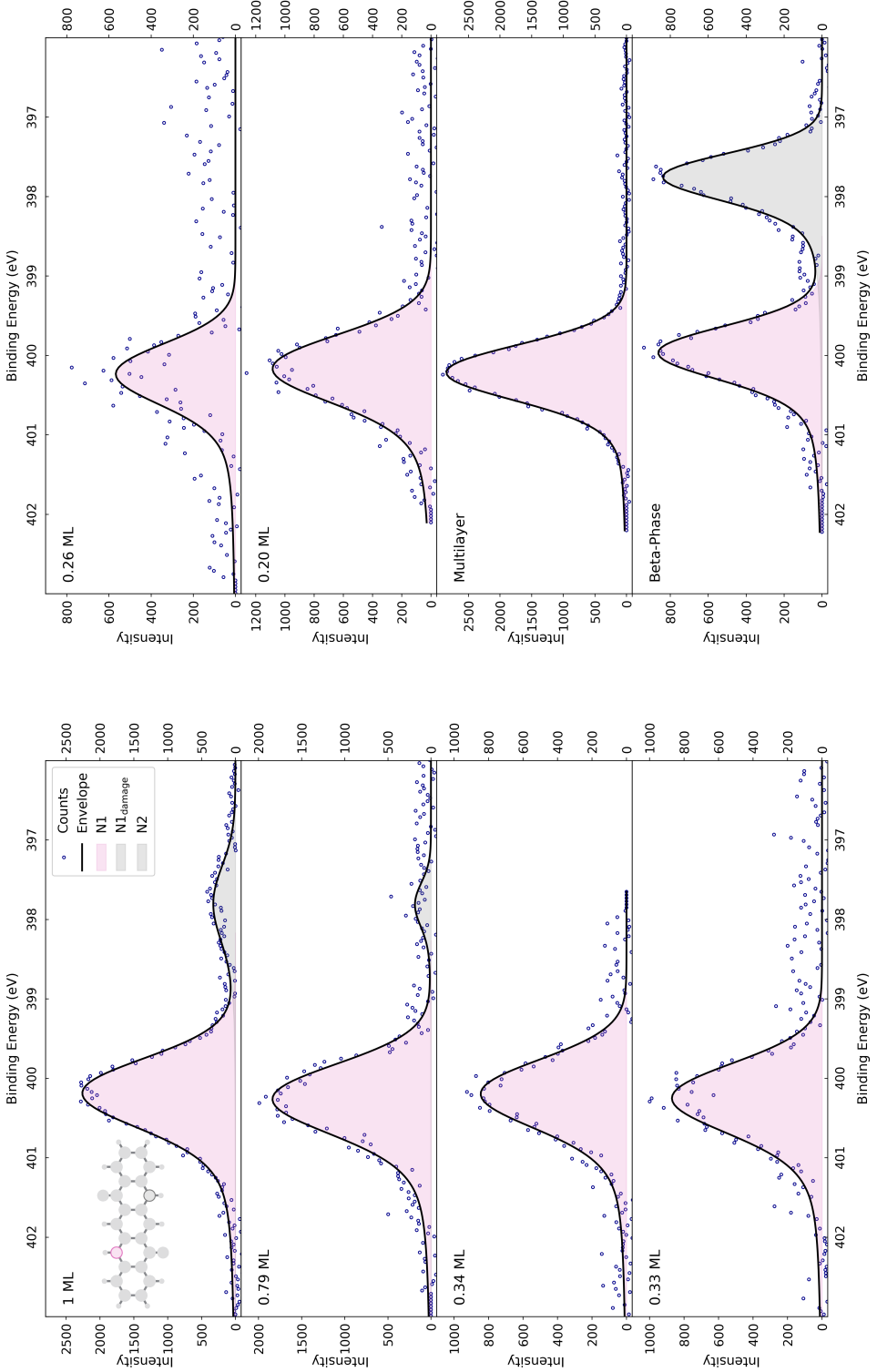


Figure 8.3: Collection of all N1s core-level XPS spectra with the different fitted peaks of all performed experiments. Each spectrum corresponds to a different preparation. The coverage of the first spectrum is set to 1 ML.

## List of abbreviations

**Ag** silver

**BE** binding energy

**fcc** face-centered cubic

**FWHM** Full Width at Half Maximum

**ML** monolayer

**NIXSW** normal incidence x-ray standing wavefield absorption

**OFET** organic field-effect transistor

**OLED** organic light-emitting diode

**OPV** organic photovoltaic

**POL** point-on-line

**PTCDA** perylenetetracarboxylic dianhydride

**QA** quinachridone

**SPA-LEED** spot profile analysis low energy electron diffraction

**STM** scanning tunneling microscopy

**UHV** ultra-high vacuum

**XPS** x-ray photoelectron spectroscopy

# Bibliography

- [1] UK Research and Innovation. *Surface Science*. Ed. by UK Research and Innovation. Sept. 2023. URL: <https://www.ukri.org/what-we-do/our-main-funds-and-areas-of-support/browse-our-areas-of-investment-and-support/surface-science/>.
- [2] The International Union for Vacuum Science, Technique, and Applications. *Surface Science*. Ed. by The International Union for Vacuum Science, Technique, and Applications. Sept. 2023.
- [3] V. Abdulrazzaq Omar A. et al. “Organic Solar Cells: A Review of Materials, Limitations an Possibilities for Improvement.” In: *Part. Sci. Technol.* 31.5 (2013), pp. 427–442.
- [4] G.A.Chamberlain. “Organic solar cells: A review.” In: *Sol. Cells* 8.1 (1983), pp. 47–83.
- [5] M. A. Green et al. “Research: Short Communication: Accelerated Publication.” In: *Progress in Photovoltaics: Research and Applications* 19.1 (2010), pp. 84–92.
- [6] Erich F. Paulus, Frank J. J. Leusen, and Martin U. Schmidt. “Crystal structures of quinacridones.” In: *Royal Society of Chemistry* 9 (2007), pp. 131–143.
- [7] Thorsten Wagner et al. “Quinacridone on Ag(111): Hydrogen Bonding versus Chirality.” In: *The Journal of Physical Chemistry C* 118.20 (2014). PMID: 24883168, pp. 10911–10920.
- [8] Alexander Richard Eberle. “Growing low-dimensional supramolecular crystals via Organic Solid-Solid Wetting Deposition.” 2019.
- [9] Frank Trixler et al. “Supramolecular Self-Assembly Initiated by Solid–Solid Wetting.” In: *Chemistry – A European Journal* 13.27 (2007), pp. 7785–7790.
- [10] Hans Niklas Humberg. “One-dimensional aggregates of the organic dye quinacridone on metallic and dielectric surfaces.” PhD thesis. Universität Bonn, 2024.
- [11] Eric Daniel Glowacki et al. “Hydrogen-Bonded Semiconducting Pigments for Air-Stable Field-Effect Transistors.” In: *Advanced Materials* 25.11 (2013), pp. 1563–1569.
- [12] Eric Daniel Glowacki et al. “Intermolecular hydrogen-bonded organic semiconductors—Quinacridone versus pentacene.” In: *Applied Physics Letters* 101.2 (July 2012), p. 023305.
- [13] Chenguang Wang, Zuolun Zhang, and Yue Wang. “Quinacridone-based  $\pi$ -conjugated electronic materials.” In: *Journal of Materials Chemistry C* 4.42 (2016), pp. 9918–9936.

- [14] Jongwook Jeon et al. “Quinacridone-quinoxaline-based copolymer for organic field-effect transistors and its high-voltage logic circuit operations.” In: *Organic Electronics* 56 (2018), pp. 1–4.
- [15] Yong Jin Jeong et al. “Development of organic semiconductors based on quinacridone derivatives for organic field-effect transistors: High-voltage logic circuit applications.” In: *IEEE Journal of the Electron Devices Society* 5.3 (2017), pp. 209–213.
- [16] Yasin Kanbur et al. “High temperature-stability of organic thin-film transistors based on quinacridone pigments.” In: *Organic Electronics* 66 (2019), pp. 53–57.
- [17] Dominik Berg et al. “Quinacridone organic field effect transistors with significant stability by vacuum sublimation.” In: *Synthetic metals* 159.23-24 (2009), pp. 2599–2602.
- [18] Chenguang Wang et al. “A diphenylamino-substituted quinacridone derivative: red fluorescence based on intramolecular charge-transfer transition.” In: *RSC Advances* 6.23 (2016), pp. 19308–19313.
- [19] Hyukgi Min, In Seob Park, and Takuma Yasuda. “*cis*-Quinacridone-Based Delayed Fluorescence Emitters: Seemingly Old but Renewed Functional Luminescences.” In: *Angewandte Chemie International Edition* 60.14 (2021), pp. 7643–7648.
- [20] Marina Pilz da Cunha et al. “A triphenylamine substituted quinacridone derivative for solution processed organic light emitting diodes.” In: *Materials Chemistry and Physics* 206 (2018), pp. 56–63.
- [21] Sebastian Dunst et al. “Comparison of the solution and vacuum-processed quinacridones in homojunction photovoltaics.” In: *Monatshefte für Chemie - Chemical Monthly* 148.5 (Mar. 31, 2017), pp. 863–870.
- [22] Hyun Ah Sung et al. “Effect of conjugated 2D-side groups on quinacridone-based copolymers to adjust deep HOMO level for photovoltaics.” In: *Journal of Industrial and Engineering Chemistry* 46 (2017), pp. 304–314.
- [23] Heinrich Hertz. “Über einen Einfluss des ultravioletten Lichtes auf die electrische Entladung.” In: *Annalen der Physik* 267.8 (1887), pp. 983–1000.
- [24] Albert Einstein. “Über einen die Erzeugung und Verwandlung des Lichtes betreffenden heuristischen Gesichtspunkt.” In: (1905).
- [25] K. Kolasinski. *Surface Science: Foundations of Catalysis and Nanoscience*. John Wiley and Sons, Ltd, 2012.
- [26] Gary Attard and Colin Barnes. *Surfaces*. Oxford University Press, 2011.
- [27] D Phil Woodruff. *Modern techniques of surface science*. Cambridge university press, 2016.
- [28] David Briggs. “Practical surface analysis.” In: *Auger and X-Ray Photoelectron Spectroscopy* 1 (1990), pp. 151–152.

- [29] John F. Moulder et al. *Handbook of X-ray Photoelectron Spectroscopy*. Ed. by Jill Chastain. Perkin-Elmer Corporation, 1993.
- [30] Neal Fairley et al. “Systematic and collaborative approach to problem solving using X-ray photoelectron spectroscopy.” In: *Applied Surface Science Advances* 5 (2021), p. 100112.
- [31] U. Müller. *Anorganische Strukturchemie*. 5th ed. Vieweg+Teubner Verlag, 2006.
- [32] R. C. Weast. *CRC handbook of chemistry and physics*. 55th ed. CRC Press, 1974.
- [33] ChemicalBook. *Quinacridone*. June 2025. URL: [https://www.chemicalbook.com/ChemicalProductProperty\\_EN\\_CB2756231.htm](https://www.chemicalbook.com/ChemicalProductProperty_EN_CB2756231.htm).
- [34] ChemSpider. *Quinacridone*. June 2025. URL: <https://www.chemspider.com/Chemical-Structure.13369.html>.
- [35] National Center for Biotechnology Information. *PubChem Compound Summary for CID 13976, Cinquasia Red*. June 2025. URL: <https://pubchem.ncbi.nlm.nih.gov/compound/Cinquasia-Red>.
- [36] J. Mizuguchi, T. Sasaki, and K. Tojo. “Refinement of the crystal structure of 5,7,12,14-tetrahydro[2,3-b]-quinolinoacridine (y-form), C<sub>20</sub>H<sub>12</sub>N<sub>2</sub>O<sub>2</sub>, at 223 K.” In: *Zeitschrift für Kristallographie - New Crystal Structures* 217.1 (2002), pp. 249–250.
- [37] *Diamond Light Source: I09*. June 2025. URL: <https://www.diamond.ac.uk/Instruments/Structures-and-Surfaces/I09.html>.
- [38] Anna Juliana Kny. “Adsorption and Ordering of Merocyanines on the Ag(100) surface.” PhD thesis. Universität Bonn, 2025.
- [39] Casa Software Ltd. *CasaXPS: Processing Software for XPS, AES, SIMS and More*. 2022.
- [40] Oliver Bauer. “Surface bonding of a functionalized aromatic molecule: Adsorption configurations of PTCDA on coinage metal surfaces.” PhD thesis. Universität Bonn, 2014.
- [41] Marco Mendolicchio et al. “Theory meets experiment for unravelling the C1s X-ray photoelectron spectra of pyridine, 2-fluoropyridine, and 2,6-difluoropyridine.” In: *The Journal of Chemical Physics* 151.12 (Sept. 2019), p. 124105.
- [42] Paul S. Bagus et al. “The XPS of pyridine: A combined theoretical and experimental analysis.” In: *The Journal of Chemical Physics* 162.8 (Feb. 2025), p. 084111.
- [43] E.T. Kang, K.G. Neoh, and K.L. Tan and. “XPS studies of charge-transfer interactions in some pyridine: organic-acceptor complexes.” In: *Molecular Physics* 70.6 (1990), pp. 1057–1064.
- [44] G. Ruano et al. “Deprotonation of the amine group of Glyphosate studied by XPS and DFT.” In: *Applied Surface Science* 567 (2021), p. 150753.